



Maize and sunflower biomass estimation in southwest France using high spatial and temporal resolution remote sensing data

M. Claverie, V. Demarez, B. Duchemin, Olivier Hagolle, D. Ducrot, C. Marais Sicre, J.-F. Dejoux, M. Huc, P. Keravec, P. Béziat, et al.

► To cite this version:

M. Claverie, V. Demarez, B. Duchemin, Olivier Hagolle, D. Ducrot, et al.. Maize and sunflower biomass estimation in southwest France using high spatial and temporal resolution remote sensing data. *Remote Sensing of Environment*, Elsevier, 2012, pp.1-14. <10.1016/j.rse.2012.04.005>. <ird-00718813>

HAL Id: ird-00718813

<http://hal.ird.fr/ird-00718813>

Submitted on 12 Dec 2012

HAL is a multi-disciplinary open access archive for the deposit and dissemination of scientific research documents, whether they are published or not. The documents may come from teaching and research institutions in France or abroad, or from public or private research centers.

L'archive ouverte pluridisciplinaire **HAL**, est destinée au dépôt et à la diffusion de documents scientifiques de niveau recherche, publiés ou non, émanant des établissements d'enseignement et de recherche français ou étrangers, des laboratoires publics ou privés.

1 ***Title***

2 Maize and sunflower biomass estimation in southwest France using high spatial and temporal
3 resolution remote sensing data

4 ***Authors***

5 Claverie M.^a, Duchemin B.^a, Hagolle O.^a, Ducrot D.^a, Marais-Sicre C.^a, Dejoux J.F.^a, Huc M.^a,
6 Keravec P.^a, Béziat P.^a, Fieuzal R.^a, Ceschia E.^a and Dedieu G.^a, Demarez V.^a.

7 ^a CESBIO, Unité mixte CNES-CNRS-IRD-UPS, 18, avenue Edouard Belin, 31401 Toulouse Cedex 4,
8 France.

9 ***Corresponding author***

10 Martin Claverie
11 Centre d'Etudes Spatiales de la BIOSphère
12 Address: CESBIO, 18 Avenue Edouard Belin, 31401 Toulouse Cedex 4, FRANCE
13 Telephone: +33561558543
14 Fax: +33561558500
15 E-mail: martin.claverie@gmail.com

16

17 ***Abstract***

18 The recent availability of high spatial and temporal resolution (HSTR) remote sensing data
19 (Formosat-2, and future missions of Venùs and Sentinel-2) offers new opportunities for crop
20 monitoring. In this context, we investigated the perspective offered by coupling a simple
21 algorithm for yield estimate (SAFY) with the Formosat-2 data to estimate crop production over
22 large areas. With a limited number of input parameters, the SAFY model enables the simulation
23 of time series of green area index (GAI) and dry aboveground biomass (DAM). From 2006 to
24 2009, 95 Formosat-2 images (8 meters, 1 day revisit) were acquired for a 24×24 km² area
25 southwest of Toulouse, France. This study focused on two summer crops: irrigated maize (*Zea*
26 *mays*) and sunflower (*Helianthus annuus*). Green area index (GAI) time series were deduced
27 from Formosat-2 NDVI time series and were used to calibrate six major parameters of the SAFY
28 model. Four of those parameters (partition-to-leaf and senescence function parameters) were
29 calibrated per crop type based on the very dense 2006 Formosat-2 data set. The retrieved
30 values of these parameters were consistent with the in situ observations and a literature
31 review. Two of the major parameters of the SAFY model (emergence day and effective light-use
32 efficiency) were calibrated per field relative to crop management practices. The estimated
33 effective light-use efficiency values highlighted the distinction between the C4 (maize) and C3
34 (sunflower) plants, and were linked to the reduction of the photosynthesis rate due to water
35 stress. The model was able to reproduce a large set of GAI temporal shapes, which were related
36 to various phenological behaviours and to crop type. The biomass was well estimated (relative

37 error of 28%), especially considering that biomass measurements were not used for the
38 calibration. The grain yields were also simulated using harvest index coefficients and were
39 compared with grain yield statistics from the French Agricultural Statistics for the department of
40 Haute-Garonne. The inter-annual variation in the simulated grain yields of sunflower was
41 consistent with the reported variation. For maize, significant discrepancies were observed with
42 the reported statistics.

43

44 **1. Introduction**

45 Soil carbon sequestration has been identified by the Intergovernmental Panel on Climate
46 Change as one of the options for the mitigation of greenhouse gases (Hutchinson et al. 2004).
47 Agricultural lands cover approximately 35% of the land surfaces and through photosynthesis
48 and biomass production, agriculture can act as carbon sinks (Ceschia et al. 2010, Kutsch et al.
49 2010). However, many factors impact photosynthesis, including crop type, crop management
50 practices, soil properties and climate. Thus, crop production is highly variable in both space and
51 time. This variability should be quantified to improve the management of agricultural lands and
52 to refine regional carbon balance estimates.

53 Land surfaces have been studied for many years using remote sensing reflectances and
54 vegetation indices (Baret and Guyot 1991, Asrar et al. 1994, Moulin et al. 1998, Bastiaanssen et
55 al. 2000, Basso et al. 2001, Pinter et al. 2003, Faivre et al. 2004, Scotford and Miller 2005,
56 Duchemin et al. 2008b). Crops fields of South-West of France are often of small size and they
57 experience high temporal dynamics due to plant growth and management practices (soil tillage,
58 sowing, irrigation and harvest). Remote sensing satellites providing high frequency observations
59 at a high spatial resolution are thus well designed to monitor cropping systems. Until recently,
60 high spatial and temporal resolutions have not been attainable because of technological
61 limitations. Currently, the Formosat-2 Taiwanese satellite has the unique capability of taking
62 daily images at 8 m spatial resolution with a constant viewing angle (Chern et al. 2006). The high
63 temporal resolution of the monodirectional Formosat-2 data allows the acquisition of very

64 accurate surface reflectances and vegetation indices time series (Hagolle et al. 2008, Hagolle et
65 al. 2010).

66 Previously, only a small number of agro-meteorological studies have been performed using both
67 high spatial and temporal resolution images with constant viewing angles such as Formosat-2
68 data. Duchemin et al. (2008b) have presented a preliminary evidence of the usefulness of such
69 data for land use mapping and agricultural water management for wheat crops in Morocco.
70 Numerous studies (Courault et al. 2008, Bsaibes et al. 2009, Hadria et al. 2010, Fieuzal et al.
71 2011) have shown its utility for capturing the spatiotemporal variability of two key biophysical
72 variables: albedo and green leaf area index. Hadria et al. (2009) have demonstrated the
73 convenience of this type of data for the detection of agricultural operations such as ploughing
74 or irrigation at the beginning of the cropping season. In this study, we analysed the potential for
75 the use of high spatial and temporal resolution images to provide regular estimates of crop
76 production over large areas. We used Formosat-2 data in combination with a simple algorithm
77 for yield estimate (SAFY, Duchemin et al. 2008a).

78 Crop models were originally designed to simulate crop growth on agricultural fields where soil,
79 climate and agricultural practices were well known and spatially homogeneous. They have been
80 used in a wide range of agro-environmental issues. However, the application of crop models
81 over large areas is still challenging because the soil properties, the climatic variables and the
82 agricultural practices are highly variable in space and time (Boote et al. 1996, Moulin et al. 1998,

83 Faivre et al. 2004, de Wit et al. 2005). In confronting this challenge, we have distinguished three
84 categories of crop models:

85 i) Complex models that simulate a large set of agro-environmental variables through the
86 description of numerous coupled phenological and physiological processes, such as
87 photosynthesis, respiration, evapotranspiration and nitrogen uptake (e.g., AFRCWHEAT2,
88 CERES, Sirius, SUCROS2, STICS, SWHEAT, see Jamieson et al. 1998 and Brisson et al. 2003
89 for reviews). These models require a large number of parameters and input data. This
90 information may be available during scientific experiments, or it may be available from
91 some farmers at a local scale, but it is generally not available over large areas.

92 ii) In contrast, very simple models calculate biomass as an empirical sum of vegetation
93 indices derived from remote sensing observations (Tucker and Sellers 1986, Dong et al.
94 2003, Wessels et al. 2006). These models are all based on the light-use efficiency (LUE)
95 theory (Monteith 1977). These models are uncomplicated to parameterise over large
96 areas using time series of remote sensing data with low spatial resolution data acquired at
97 10-day or monthly intervals. They provide estimates of net primary production for natural
98 ecosystems such as forests (e.g., Dong et al. 2003) or grasslands (e.g., Tucker et al. 1983,
99 Prince 1991, Wylie et al. 1991, Loseen et al. 1995). However, these models appear less
100 suited for crop monitoring because they do not accurately account for crop type and
101 management (Faivre et al. 2004).

102 iii) The third category of crop models gathers the descriptions of the main biophysical
103 processes (biomass accumulation, leaf partition, leaf senescence,...) and empirical
104 parameterisations. These models combine the LUE theory with a simulation of the
105 successive plant phenological phases. This semi-empirical approach, in which the number
106 of formalisms and parameters is limited, enables studies over larger areas. Maas (1993)
107 has demonstrated the value of such a model for simulating time series of leaf area index
108 and dry aboveground biomass for maize and wheat crops. Lobell et al. (2003) and Liu et al.
109 (2010), who worked on the combination of such semi-empirical models and remote
110 sensing data, have underlined the need for high temporal and spatial resolution satellite
111 data to improve model predictions.

112 The SAFY model (Duchemin et al. 2008a) belongs to this third category of semi-empirical
113 models. It was specifically designed for large-scale studies because it describes the main
114 biophysical processes using climatic data. Previous studies have shown that the SAFY model,
115 once calibrated with green leaf area index time series, resulted in accurate estimates of dry
116 aboveground biomass for irrigated wheat cultivated in semi-arid regions (Duchemin et al.
117 2008b, Hadria et al. 2009, Fieuzal et al. 2011).

118 The objective of this study was to evaluate the coupling between high spatial and temporal
119 resolutions remote sensing data with a simple crop model to estimate crop production at
120 regional scale. An example is shown using Formosat-2 images combined with the SAFY model
121 applied to sunflower (*Helianthus annuus*) and maize (*Zea mays*) in southwest France. The

122 experiment was performed during four successive agricultural seasons (2006-2009) with a focus
123 on maize and sunflower crops, which are the two dominant summer crops cultivated in the
124 southwest of France. Time series of Formosat-2 observations were used to calibrate parameters
125 of the SAFY model over a region covering approximately 600 km². Evaluation of the model used
126 an in situ data set collected from 2006 to 2009 and regional grain yield statistics.

127 ***2. Material and methods***

128 ***2.1. Study area***

129 The study area is a 24 × 24 km² area located near Toulouse, in southwest France (1°10' E,
130 43°27' N, Fig. 1). The climate is temperate continental with hot (daily mean temperature
131 approximately 22.5 °C) and dry (38 mm/month of rainfall) summers. Arable lands cover up to
132 60% of the study area, of which 40% is cultivated during summer, predominantly with irrigated
133 maize (grain and silage) and sunflower crops. The southeastern and the western parts of the
134 study area are hilly landscapes with small fields (approximately 10 ha); the centre of the study
135 area, near the Garonne River, is nearly flat with larger fields (approximately 25 ha).

136 In the study area, maize fields are sown from mid-April to beginning of June, and last until
137 September-October. Most of maize fields are irrigated during hottest month (July and August).

138 Sunflower fields are sown from end of March to end of June and are mainly non-irrigated.

139 **2.2. *Field data***

140 The study was performed during from 2006 to 2009 on maize and sunflower crops. Four types
141 of in situ data were measured: the dry aboveground biomass (DAM), the green area index (GAI)
142 and the fraction of absorbed photosynthetically active radiation (FAPAR). The DAM and the SLA
143 were estimated with a destructive method. The GAI and the FAPAR were estimated from
144 hemispherical photographs.

145 The main characteristics of the field measurements are shown in Fig. 1 and Table 1. Two
146 protocols were used to collect the data:

147 (i) Transect sampling protocol: the measurements of DAM were performed from 2006 to
148 2008 along two transects crossing the field. This protocol was applied in two fields
149 belonging to the CarboEurope-IP Regional experiment (Dolman et al. 2006). These two
150 fields are hereafter referred to as “Lamothe” and “Auradé”. They belong to an
151 experimental farm managed by the Purpan Engineering School and to a farmers
152 association (<http://www.agriculteurs-aurade.fr/>). Thirty plants were harvested 6 to 9
153 times per growing season (Table 1). For each plant, leaf biomasses were measured
154 independently and leaf areas were measured using a planimeter (Licor 3100 Lincoln Inc.,
155 Nebraska) in order to derive the specific leaf area (SLA).

156 (ii) Elementary sampling unit (ESU) protocol: the measurements of DAM, GAI and FAPAR
157 were performed within a 20 m sided square area. Eleven fields located near the
158 “Lamothe” farm were sampled (back squares in Fig. 1 and Table 1). These fields are

159 hereafter referred to as the ESU fields. The locations of the ESUs were recorded with a
160 GPS. GAI and FAPAR were measured in 2008 using digital hemispherical photographs
161 (DHPs). Each ESU was sampled with 13 DHPs applying the VALERI spatial sampling
162 protocol (<http://w3.avignon.inra.fr/valeri>). The in situ data were collected 7 to 10 times
163 during the growing season yielding 23 GAI and FAPAR estimations for maize and 19 for
164 sunflower (Table 1). The DAM was estimated from 10 plants collected near the ESUs in
165 2008 and 2009, leading to 14 DAM estimations for maize and 11 for sunflower. In 2009,
166 only one biomass measurement was performed per ESU during the growing season.

167 The concept of green area index (GAI, Baret et al. 2010) corresponds to the photosynthetically
168 active plant area without organ distinctions. It is related to FAPAR and can be derived from
169 DHPs. In our study, the DHPs were taken with a Nikon CoolPix 8400 camera equipped with a FC-
170 E8 fisheye lens. The camera was put at the top of a pole to keep the viewing direction (looking
171 downward) and the canopy-to-sensor distance constant (~1.5m) throughout the growing
172 season. This protocol allowed the reduction of errors in the directional gap fraction estimates
173 and thus in the FAPAR and GAI estimates (Demarez et al. 2008). The DHP were processed using
174 CAN-EYE V5 (<http://www4.paca.inra.fr/can-eye>), which provides estimates of the daily FAPAR
175 and of the "effective" and "true" GAI (Demarez et al. 2008, Baret et al. 2010). In this study, we
176 used the effective GAI ($GAI_{\text{eff,CAN-EYE}}$), which is highly correlated with remote sensing
177 observations and the daily FAPAR ($FAPAR_{\text{daily,CAN-EYE}}$).

178 In addition to these measurements, several farmers provided grain yield estimates for maize (4
179 estimates) and sunflower (37 estimates) for 12 fields located near Lamothe and for 16 fields
180 located near Auradé (blue disks in Fig. 1).

181 **2.3. Meteorological data**

182 Meteorological data were generated by the mesoscale atmospheric analysis system SAFRAN,
183 which is operational at Météo-France (Durand et al. 1993). Among other variables, SAFRAN
184 simulates air temperature at 2 m above the ground (T_a), incoming global radiation (R_g) and
185 precipitation (P) based on a combination of measurements (weather stations) and modelling.
186 The data are available every 6 hours over a grid with an 8 km spatial resolution (plus symbols in
187 Fig. 1).

188 The SAFRAN meteorological variable data were processed to compute daily mean T_a and
189 cumulated daily R_g and P for each Formosat-2 pixel (8 meters) of the study area. The spatial
190 oversampling was performed using a bilinear spatial interpolation.

191 The evaluation performed by Quintana-Segui et al. (2008) all over the France have shown that
192 R_g (RRMSE = 60%) and T_a (RRMSE = 13%) are accurately estimated by SAFRAN, while the
193 accuracy of P was found lower (RRMSE = 100%), especially in mountainous areas.

194 The analysis of the meteorological variables over the Formosat-2 footprint revealed differences
195 between the years. The driest and hottest years were 2006 and 2009; the cumulated daily
196 precipitation for the summer growing season, from DoY (day of year) 125 to 250, was 147 mm

197 in 2006 and 152 mm in 2009, whereas it reached 248 mm in 2008 and 273 mm in 2007. The
198 cumulated air temperature during the same period was approximately 2570 °C in 2006 and
199 2009 and approximately 2370 °C in 2007 and 2008.

200 **2.4. Formosat-2 data**

201 Formosat-2 is a high spatial (8 meters) and temporal (daily revisit time) resolution satellite with
202 four spectral bands (488, 555, 650 and 830 nm) and a 24 km field of view (Chern et al. 2006).
203 Formosat-2 takes images at a constant viewing angle. Ninety-Five images were taken of our
204 study area from 2006 to 2009 (Fig. 2). In 2006, the images were scheduled at a high priority
205 level with a nominal time step of 3 days. The 2006 data set contained 51 images, including 27
206 images that were almost totally cloud-free. After 2006, only images with a cloud cover less than
207 20% were purchased. Thus, 14 images were available in 2007, 11 images in 2008 and 19 in 2009.
208 In 2008, no cloud-free images were available from February 11 to June 19.
209 All of the Formosat-2 images were pre-processed for geometric, radiometric and atmospheric
210 corrections and the filtering of clouds and shadows (Hagolle et al. 2008, Hagolle et al. 2010).
211 This processing resulted in surface reflectances images and associated cloud-masks. The
212 absolute location accuracy was 0.4 pixels, i.e., 3.2 m (Baillarin et al. 2008), which is quite
213 satisfactory with respect to both the field and ESU sizes.

214 **2.5. Land cover**

215 Maize and sunflower were identified using classification and segmentation methods applied to
216 Formosat-2 surface reflectances images. This processing was performed each year using all
217 images acquired from January to December. The classification method was performed using a
218 fuzzy contextual algorithm of the Iterative Conditional Mode type based on a Markovian model
219 (Idbraim et al. 2009). The segmentation algorithm was based on a watershed method (Fjortoft
220 et al. 1999) and led to homogenous units (called HU hereafter), corresponding to
221 homogenous radiometric zones. The parameters used for the segmentation were chosen such
222 that the agricultural fields were split in the case of high intra-field variability. As a result, an
223 agricultural field corresponded to one or several HU (see Fig. 3). Only HU larger than 640 m² (10
224 Formosat-2 pixels) and covered by a minimum of 80% of either maize or sunflower pixels were
225 considered in this study.

226 Each year, this processing provided 40 land use classes, from which maize (grain and silage) and
227 sunflower were extracted. The analysis of the mapped HU showed that:

228 (i) Sunflower and maize crops covered approximately 21% of the study area.

229 (ii) Maize was primarily cultivated in the centre of the Formosat-2 images, near the
230 Garonne River. It covered approximately 7700 ha in 2006, 6500 ha in 2007, 7400 ha in
231 2008 and 6600 ha in 2009. The maize crops were segmented into HU of 2 ha on average.
232 Approximately 95% of these HU were identified as grain maize, the remaining 5% being
233 silage maize.

234 (ii) Sunflower was cultivated throughout the study area and was dominant over the hill
235 landscapes at the eastern and western part of the study area. Sunflower crops covered
236 approximately 6300 ha in 2006, 5100 ha in 2007, 7200 ha in 2008 and 7200 ha in 2009.
237 Sunflower was segmented into smaller HU than maize of approximately 0.7 ha on average.
238 This was expected as sunflower crops were not irrigated and were often cultivated on
239 hills. Thus, these crops exhibited a higher intra-field variability due to the variation in soil
240 properties and water availability.

241 **2.6. Time series of Green Area Index (GAI)**

242 Many studies have demonstrated the link between spectral vegetation indices (e.g., NDVI, SAVI
243 and EVI) derived from remote sensing observations and the green leaf area index (e.g., Myneni
244 1994, Weiss et al. 2002, Colombo et al. 2003, Walthall 2004, Duchemin et al. 2006). In our study,
245 the green area index ($GAI_{\text{eff},F2}$) was estimated from the Formosat-2 images using the NDVI and
246 the following exponential relationship (Eq. 1):

$$247 \quad GAI_{\text{eff},F2} = k_1 \times e^{k_2 \times NDVI} - k_3 \quad (1)$$

248 The coefficients of Eq. 1 were estimated using the minimisation of the root mean square error
249 (RMSE) between $GAI_{\text{eff},CAN-EYE}$ estimated from the DHPs from the ESUs and $GAI_{\text{eff},F2}$ estimated
250 from Eq. 1. The $GAI_{\text{eff},CAN-EYE}$ measurements taken more than 4 days after or before the
251 Formosat-2 acquisitions were eliminated from the data set. The NDVI- $GAI_{\text{eff},CAN-EYE}$ scatterplot is
252 presented in Fig. 4. A single relationship (the black line in Fig. 4) was used for both crops

253 (coefficients $k_1=0.35$, $k_2=2.86$, $k_3=0.24$ in Eq. 1). The RMSE between $GAI_{\text{eff,CAN-EYE}}$ and $GAI_{\text{eff,F2}}$ was
254 equal to $0.38 \text{ m}^2 \cdot \text{m}^{-2}$ and the relative RMSE (RRMSE) was equal to 20%. The formulation of the
255 equation differed from more commonly used logarithmic formulation. Nevertheless, the current
256 formulation fitted correctly with the in situ measurements of effective GAI. With the current set
257 of coefficients, the GAI estimate could not exceed $5.9 \text{ m}^2 \cdot \text{m}^{-2}$, which was sufficient as it
258 corresponded to effective GAI.

259 This relationship was then applied to all Formosat-2 pixels. This processing resulted in a time
260 series of effective Formosat-2 GAI (called hereinafter GAI_{F2}), which were spatially averaged over
261 the HU labelled as maize (silage or grain) and sunflower. During the calculation, all of the data
262 with cloudy or shadowed pixels were excluded.

263 ***2.7. Calibration of the SAFY model***

264 The simple algorithm for yield estimates (SAFY) is a daily time step model that simulates time
265 series of leaf area index and dry aboveground biomass from the air temperature and the global
266 incoming radiation. An overview of the model is provided in the Appendix 1; a full description is
267 available in Duchemin et al. (2008a).

268 The model was parameterised for each HU labelled as maize (silage or grain) or sunflower using
269 meteorological data derived from SAFRAN. The thirteen parameters of the SAFY model are
270 listed in Table 2. Initial values were put based on a literature review and field measurements for

271 eight parameter and the six major parameters, identified by Duchemin et al. (2008a), were
272 calibrated using only time series of green area index derived from Formosat-2 images (GAI_{F2}).

273 ***2.7.1. Calibration of parameters through literature review and field*** 274 ***measurements***

275 The common value of 0.48 was used for the climatic efficiency (Varlet-Grancher et al. 1982). As
276 in Duchemin et al. (2008a), the initial dry aboveground biomass was set arbitrarily to
277 correspond with a GAI of $0.1 \text{ m}^2 \cdot \text{m}^{-2}$.

278 The three critical temperature values (T_{\min} , T_{\max} , T_{opt} , Eq. 3 in the Appendix 1) and the degree of
279 the polynomial function (β) that defines the stress temperature function for each crop were
280 obtained from Drouet and Pages (2003) and from the STICS website
281 (http://www.avignon.inra.fr/agroclim_stics/).

282 The light-extinction coefficient (k_{ext}) was computed by inverting Beer's law (Eq. 5 in the
283 Appendix 1) using the fraction of absorbed photosynthetically active radiation ($FAPAR_{\text{daily,CAN-EYE}}$)
284 and the effective green area index ($GAI_{\text{eff,CAN-EYE}}$) from CAN-EYE. The specific leaf area (SLA) were
285 estimated from measurements of leaf biomass and leaf area done at Lamothe in 2006 (maize)
286 and at Auradé in 2007 (sunflower). Only measurements before the maximum GAI were
287 considerate.

288 ***2.7.2. Calibration of parameters based on remote sensing data***

289 The remaining parameters (Pl_a , Pl_b , Stt , Rs , D_0 and $ELUE$) were all retrieved using only GAI_{F2} time
290 series derived from Formosat-2 images. To limit compensation during the optimisation
291 procedure (see Duchemin et al. 2008a), we classified the parameters in two groups: crop-
292 specific and field-specific parameters. Two corresponding phases were used for the calibration.
293 The methodology of the calibration is described in the Fig. 5. The four crop specific parameters
294 (Pl_a , Pl_b , Stt , Rs), which constrain the shape of the GAI_{F2} time course, were calibrated, on phase
295 1, separately for sunflower, grain maize and silage maize. The two field specific parameters (D_0
296 and $ELUE$) were calibrated, on phase 2, for each HU.

297 Prior to the calibration procedure, a delimitation of the growing period was needed (Fig. 6). The
298 day of maximum GAI_{F2} (DoY 218 in Fig. 6) was first identified. The algorithm then seeks
299 backward from this day to determine the starting day of the growing period (DoY 156 in Fig. 6),
300 which was defined as the day that exhibited a GAI_{F2} value less than a user-defined threshold.
301 This threshold was set as the minimum GAI_{F2} value, encountered in the backward seek, plus 0.1.
302 The end of the growing season (DoY 288 in Fig. 6) was identified in a similar way, seeking
303 forward before the day of maximum GAI_{F2} . The GAI_{F2} values that did not belong to the identified
304 growing period were excluded (plus symbols in Fig. 6).

305 The calibration of SAFY was then performed by minimising the Root Mean Square Error (RMSE)
306 between the “cleaned” GAI_{F2} time series and the GAI simulated by SAFY. The minimisation
307 procedure was based on an adapted version of the simplex method (Lagarias et al. 1998), which
308 was run 50 times with a random determination of initial values to avoid stops in local minima.

309 Intervals of acceptable values were defined for each parameter (Table 2). These intervals were
310 constant for all of the parameters except the date of emergence, for which the interval was
311 established independently for each HU to plus or minus 20 days around the start of the growing
312 period.

313 The crop-specific parameters were estimated, on phase 1 of the calibration (see Fig. 5), using
314 the GAI_{F2} time series of the 6032 HU deduced from the 2006 Formosat-2 data set. This data set
315 was preferred as it contained a high number of images regularly distributed during the whole
316 growing season. Depending on the HU, 18 to 28 cloud-free images were available from May to
317 September. HU with maximum GAI_{F2} less than $1 \text{ m}^2 \cdot \text{m}^{-2}$ or that lead to RMSE superior to 0.38
318 $\text{m}^2 \cdot \text{m}^{-2}$ were not kept in our analysis as they were considered to be incorrectly classified.
319 However, an important set (95 %) of crop-specific parameters (Pl_a , Pl_b , Stt , Rs) was available for
320 each crop: 1980 for grain maize, 97 for silage maize and 3644 for sunflower. A median value was
321 then computed for each crop and used on phase 2 of the calibration (see Fig. 5) to constrain the
322 estimation the field-specific parameters (D_0 and $ELUE$). These latter parameters were estimated
323 per year and per spatial pattern: HU for Formosat-2 footprint estimates, and transect, ESU and
324 field for local estimates. The minimisation procedure of phase 2 was based on a regular simplex
325 method because there is no compensation between these two parameters (Duchemin et al.
326 2008a).

327 ***3. Results and discussion***

328 In this section, results of the calibration and the validation are discussed. The two parameters,
329 estimated from in situ measurements are first discussed. The parameters, estimated from the
330 GAI_{F2} are then described: crop-specific (Pl_a , Pl_b , Stt and Rs) and field-specific ($ELUE$ and D_0).
331 Finally, the validations at local and regional scales are described in the two last sections.

332 **3.1. *Light-extinction coefficient and Specific Leaf Area***

333 Fig. 7 displays the relationship between the fraction of absorbed photosynthetically active
334 radiation ($FAPAR_{daily,CAN-EYE}$) and the effective green area index ($GAI_{eff,CAN-EYE}$). A single
335 relationship was used for both crops. The best agreement was obtained using a light-extinction
336 coefficient (K_{ext}) of 0.63 (see Eq. 5 in the Appendix 1). The RMSE between FAPAR derived from
337 this relationship and $FAPAR_{daily,CAN-EYE}$ was 0.033.

338 The relationship between the leaf area and leaf mass is displayed in Fig. 8. These two variables
339 were linearly related. SLA values corresponding to the slopes of the relationships (Fig. 8) were
340 used in the SAFY simulations: $0.012 \text{ m}^2 \cdot \text{g}^{-1}$ for sunflower and $0.024 \text{ m}^2 \cdot \text{g}^{-1}$ for maize.

341 **3.2. *Crop-specific parameters***

342 Fig. 9 shows the box and whiskers plots of the distributions of the crop specific parameters (Pl_a ,
343 Pl_b , Stt and Rs) for maize (grain: M and silage: SM) and sunflower (SF) based on phase 1 of the
344 calibration applied on the 5721 HU of the 2006 Formosat-2 data set. Their median values are
345 reported in Table 2 and the distributions appeared very scattered. As previously suggested by

346 Duchemin et al. (2008a), part of this scattering can be attributed to parameter compensations
347 occurring during the minimisation procedure. The parameters appeared more scattered for
348 sunflower than for maize likely because sunflower crops, which are not irrigated, are much
349 more sensitive to the spatial distribution of rainfall and to soil water content than is maize. They
350 thus experienced larger variations in the GAI_{F2} time series.

351 “Typical” maize (grain and silage) and sunflower GAI_{F2} time series computed from three HU of
352 the 2006 Formosat-2 data set are plotted on Fig. 10. The analysis of Fig. 9, Fig. 10 and Table 2
353 revealed that significant information could be derived from the distributions of the crop specific
354 parameters:

355 (i) The dry aboveground biomass allocated to the leaf at plant emergence ($1-Pl_a$) was 65%
356 for grain maize, 66% for silage maize and 84% for sunflower (Fig. 9). These values were
357 consistent with the ratios of the leaf mass to the dry aboveground biomass derived from
358 *in situ* measurements at the beginning of the agricultural season, which were 75% for
359 maize (Lamothe in 2006) and 83% for sunflower (Auradé in 2007).

360 (ii) No significant difference was observed between the grain and silage parameters,
361 except the rate of senescence (R_s in Table 2), which was approximately 15 times higher for
362 silage maize. This very high rate of senescence for silage maize corresponded with the
363 sudden drop of GAI_{F2} due to harvesting as illustrated in Fig. 10. Silage maize is used to feed
364 animals and thus it is harvested earlier than grain maize, when grain humidity reaches
365 80%.

366 (iii) Senescence began earlier for sunflower than for maize. The threshold of cumulated
367 temperature to initiate senescence was estimated to be 70% lower for sunflower than for
368 maize (Stt in Table 2). This difference is well illustrated in the GAI_{F_2} time series (Fig. 10)
369 and was previously shown by Andrade (1995).

370 **3.3. Field specific parameters**

371 The cumulated distribution of the effective light-use efficiency (ELUE) and the emergence dates
372 (D_0) estimated for the sunflower and maize crops of the Formosat-2 footprint are presented in
373 Fig. 11 (a to d). Numbers of HU used to compute the cumulated distribution are shown in the
374 Fig. 11 (a and b). The cumulated distributions of the maximum GAI (GAI_{max}), the rainfall and the
375 temperature stress factor are also plotted (Fig. 11 e to j). The rainfall was cumulated from 30
376 days before emergence to senescence. The temperature stress factor corresponds to the
377 average of the F_T function (Eq. 3 in the Appendix 1) from emergence to senescence.

378 The median value of the ELUE averaged over the four years was 3.3 g.MJ^{-1} for maize (Fig. 11a)
379 and 2.0 g.MJ^{-1} for sunflower (Fig. 11b). The SAFY model thus appeared adequate to reproduce
380 the basic difference in photosynthetic rate between maize (C4 plant) and sunflower (C3 plant).
381 The ELUE values for sunflower increased from 2006 to 2008 in relation with the increasing
382 values of cumulated rainfall (Fig. 11h). This is consistent as this parameter is expected to include
383 water stress effect. A similar positive correlation was observed between the median values of
384 cumulated rainfall and GAI_{max} (Fig. 11f). In contrast, the inter-annual variation in maize ELUE was
385 not related to the rainfall. This is consistent as maize is irrigated to avoid water stress. The

386 analysis of the distribution of GAI_{max} (Fig. 11e) permitted the explanation of the inter-annual
387 maize ELUE variations. In 2006 and 2009, the GAI_{max} values were similar despite differences in
388 temperature stress factors, which were highest in 2009 (Fig. 11i). Thus, the calibration
389 procedure induced highest ELUE values in 2009 (Fig. 11a) to compensate for the negative effect
390 of low temperatures on GAI. The same trend was observed in 2007 and 2008; the highest values
391 of temperature stress factor and ELUE were found in 2007. These results revealed that the
392 GAI_{max} is a good indicator of water or temperature stresses and that the model and the
393 calibration procedure proposed here were able to reproduce such effects.

394 The emergence dates (D_0) were also significantly different between maize (Fig. 11c) and
395 sunflower (Fig. 11d). For maize, the median value was stable over the years and was
396 approximately 164 (June, 13). The plant emergence always occurred within a limited time
397 period; each year, 90% of all of the D_0 values were within +/- 15 days of the annual median
398 value. For sunflower, D_0 was more variable and 90% of the D_0 values were within +/- 45 days of
399 the annual median value. This was consistent with difference in irrigation between the crops;
400 sunflower is not irrigated and thus is more sensitive to the spatial variability of rainfall events
401 and soil properties, which may induce strong differences between fields.

402 ***3.4. Evaluation of the simulated GAI and DAM time series at local*** 403 ***scale***

404 A quantitative evaluation of the model was performed by comparing the dry aboveground
405 biomass (DAM) simulated by SAFY with those estimated from field measurements. The spatial
406 pattern used for the validation corresponded to the footprint of in situ data: transect, ESU and
407 field. The model was calibrated using the GAI_{F2} time series averaged over the pixels that
408 encompassed transects (sunflower at Auradé in 2007 and maize at Lamothe in 2006 and 2008),
409 over a 3x3 pixel window centred on the ESUs (2008 and 2009) or over the pixels that
410 encompassed fields where grain yields were collected. The GAI_{F2} and DAM time series from
411 2006 to 2008 resulting from this processing are displayed in Fig. 12.

412 The analysis of the simulated GAI time series confirmed that the SAFY model was able, after
413 calibration, to reproduce the large range of the observed GAI_{F2} shapes. The maximum GAI_{F2}
414 values of maize were quite low ($< 3.5 \text{ m}^2 \cdot \text{m}^{-2}$), which is expected as effective values are proven
415 to underestimate destructive values. This underestimation could reach 30% for the maize and
416 16% for the sunflower as shown by Demarez et al. (2008). The continuous GAI increase during
417 leaf growth appeared to be accurately reproduced for all of the crops. The difference observed
418 in the time duration of maximal GAI between the sunflower and the maize is also well
419 reproduced. Finally, the GAI decrease during the senescence period was correctly simulated for
420 all crops except for the sunflower crop in 2008 (case 6, Fig. 12); the observed sudden decrease
421 was not simulated by the SAFY model. Hemispherical photographs (Fig. 13) taken in 2008 on July
422 17 and 24 (referred to as A and B in Fig. 12) revealed that the NDVI and GAI decrease
423 corresponded with flowering.

424 The temporal dynamics of DAM were correctly reproduced in most of cases. Most of the
425 simulated values ranged within the averages plus or minus the standard deviation of the field
426 measurements. However, some discrepancies were noted:

427 (i) In 2008, the maximum DAM produced by the grain maize (case 3, Fig. 12) was
428 underestimated by approximately 29% in relative terms. The deviation may be explained
429 by the lack of consideration of an increase of the light use efficiency (LUE) allocated to
430 shoot biomass at the end of the cycle, due to the cessation of root growth. At the
431 opposite, the simulated LUE ($F_T \times ELUE$) decreases from September as the air temperature
432 decreases.

433 (ii) In contrast with maize, the maximum DAM produced by sunflower (cases 4 and 6 in
434 Fig. 12) were overestimated. The maximum dry aboveground biomass was unfortunately
435 not measured for case 5. Recent work by Lecoeur et al. (2011) performed with similar
436 sunflower varieties showed that ELUE decreases from the flowering phase, probably in
437 favour of lipids production. The slight decrease in DAM observed before senescence in the
438 measured biomass was due to measurement errors.

439 The global comparison between simulated and measured DAM from 2006 to 2009 is presented
440 on Fig.14 and Table 3. There is a good agreement between simulations and field
441 measurements, with a high correlation ($r^2 = 0.92$, $p\text{-value} < 0.001$), almost no bias ($- 0.02 \text{ kg.m}^{-2}$)
442 and an error (RMSE) of 0.21 kg.m^{-2} . The correlation is higher for silage maize ($r^2 = 0.96$; RRMSE =
443 11%) than for grain maize ($r^2 = 0.86$; RRMSE = 26%) and sunflower ($r^2 = 0.78$; RRMSE = 39%). The

444 global accuracy of simulations (RRMSE = 28% on Fig. 14) was satisfactory considering that the
445 most sensitive parameters of the model were only calibrated with remote sensing observations.
446 This accuracy was comparable to that of studies using more complex models with a large in situ
447 data set. They found accuracy of 14% and 32% for maize using SWATRER-SUCROS and CERES
448 (Xevi et al. 1996), 16% using STICS (Brisson et al. 2002) and 23% using EPIC (Cabelguenne et al.
449 1999). An accuracy of 21% was found for sunflower using EPIC (Cabelguenne et al. 1999).

450 The SAFY model was also run for fields for which farmers provided grain yields. The in situ grain
451 yields were compared with the maximum simulated DAM (Fig. 15). The data for sunflower were
452 highly scattered. This was partially due to the overestimations of the SAFY biomass and partially
453 due to uncertainties in the in situ grain yields. For maize, too few measurements were available
454 to exhibit a trend. Despite these limitations, a mean harvest index (HI) was computed for each
455 crop as the ratio of in situ grain yields to the maximum DAM. This index was 0.48 for grain maize
456 and 0.25 for sunflower. The HI calculated for maize appeared consistent with those from
457 previous experimental or modelling studies; Cabelguenne et. al (1999) reported a value of 0.5.
458 Due to the SAFY biomass overestimation, the HI calculated for sunflower was very low
459 compared with the in situ values given by Casadebaig (2008), which varied between 0.35 and
460 0.45.

461 ***3.5. Evaluation of the simulated DAM and grain yield over the*** 462 ***Formosat-2 footprint***

463 The distributions of the maximum aerial dry biomass (DAM_{max}) estimated over the whole
464 Formosat-2 footprint are presented in Fig. 16. For sunflower, the maximum DAM values (Fig.
465 16b) were reached during the wettest year (2008, Fig. 11h). In 2007, despite the strong rainfall,
466 the DAM_{max} values were not as high as in 2008. In 2007, we noticed that the period of
467 emergence was quite long, up to 200 days (Fig. 11d). This was due to heavy rains during the
468 spring, which limited plant emergence, particularly in clay soils, and thus limited the crop
469 production. For maize, the highest maximum DAM values were reached during the hottest years
470 (Fig. 11i).

471 The DAM_{max} values averaged over four years were equal to approximately $19.5 \text{ t}\cdot\text{ha}^{-1}$ for maize
472 and $9.6 \text{ t}\cdot\text{ha}^{-1}$ for sunflower. The grain yields calculated from these averaged DAM_{max} values
473 using the harvest index previously estimated (0.48 for maize and 0.25 for sunflower) were 10.1
474 $\text{t}\cdot\text{ha}^{-1}$ for maize and $2.4 \text{ t}\cdot\text{ha}^{-1}$ for sunflower and were in agreement with the values given by the
475 French Agricultural Statistics for the whole department of Haute-Garonne, which were $10.2 \text{ t}\cdot\text{ha}^{-1}$
476 1 for maize and $2.3 \text{ t}\cdot\text{ha}^{-1}$ for sunflower (Fig. 17, Agreste 2011). The accuracy of the sunflower
477 grain yield estimation was due to compensation between the overestimated biomass and the
478 underestimated harvest index. Nevertheless, the inter-annual variations of the estimated
479 sunflower grain yields were highly correlated with the reported statistics ($r = 0.97$, $p\text{-value} < 0.03$,
480 Fig. 17). The lowest simulated grain yields were found in 2006 which was the driest year (Fig.
481 11h) like in the reported statistics; the highest simulated grain yields were found in 2008 which
482 was the wettest year like in the reported statistics.

483 In contrast with sunflower, the inter-annual variation in the maize grain yields did not match the
484 reported grain yield statistics ($r = -0.81$, Fig. 17). The lowest simulated grain yields were found in
485 2008, which was the year with the highest reported grain yields. The highest simulated grain
486 yields were estimated for 2009, which had the lowest reported grain yields. As discussed
487 previously, there was a clear effect of temperature on maize leaf and biomass production. We
488 may notice that the reported statistics are given for the entire department of Haute-Garonne,
489 which covers an area much larger than the Formosat-2 footprint. In contrast with the sunflower
490 crops, which are mainly located in the northern part of the department, the maize crops are
491 distributed throughout the department, which exhibits a strong spatial gradient in air
492 temperatures. The mean air temperatures were cumulated during the growing period using the
493 SAFRAN data. They varied from 2419 °C (in 2007) to 2646 °C (in 2006) in the northern part of the
494 department and from 2001 °C (in 2007) to 2202 °C (in 2006) in the southern part of the
495 department. The differences observed in cumulative temperature between the northern and
496 the southern part of the department could reach 400 °C. The Formosat-2 footprint was located
497 in the northern part of the department with a cumulative air temperature varying from 2353 °C
498 (in 2007) to 2600 °C (in 2006). Thus, the SAFY simulations performed over the maize crops were
499 considered to not be representative of the entire department of Haute-Garonne and thus
500 unfortunately not comparable with the reported statistics.

501 ***4. Conclusion***

502 In this study, we evaluated the combined use of high spatial and temporal resolutions remote
503 sensing data and a simple crop model to estimate maize and sunflower crops production. A
504 semi-empirical crop model (SAFY, Duchemin et al. 2008a) was calibrated with high temporal and
505 spatial resolution Formosat-2 data available from 4 years (2006 to 2009). The results revealed
506 that the high frequency of the 2006 Formosat-2 data set (27 cloud free images throughout the
507 year) permitted the estimation of phenological parameters (Pl_a , pl_b , Stt and Rs), which were
508 proven to be crop dependant. Once calibrated, these parameters were used to calibrate
509 effective light-use efficiency (ELUE) and emergence dates (D_0), and to simulate biomass from
510 2006 to 2009. From 2007 to 2009, fewer images were available, but the method remained
511 robust because it relied on the pre-calibration of the phenological parameters using the 2006
512 high temporal resolution data set. Analysis of the ELUE values showed that the SAFY model was
513 able to reproduce the basic difference in photosynthetic rate between maize (C4 plant) and
514 sunflower (C3 plant). The simulation of D_0 revealed higher variability of non-irrigated sunflower
515 than irrigated maize. The SAFY model was also able to reproduce the temporal variability of
516 GAI_{F2} shape and dry aboveground biomass through the 4 studied years. The errors retrieved
517 from the comparison between destructive sampling and simulated biomass were consistent
518 ($RMSE = 0.22 \text{ kg.m}^{-2}$; $RRMSE = 29\%$) in comparison with the values given by authors who used
519 more complex models. However, this approach faced some limitations. First, the use of the
520 2006 Formosat-2 data set to calibrate phenological parameters (Pl_a , pl_b , Stt and Rs) is a potential
521 source of error. Indeed, the unusual hot at dry meteorological conditions of 2006 impacted the
522 value of calibrated parameters and, thus, all estimations of biomass. Secondly, in the SAFY

523 model, the ELUE is constant over the phenological cycle, which could lead to errors in the dry
524 aboveground biomass estimations. For example, Lecoecur et al. (2011) showed that the ELUE of
525 sunflower decreased during the maturity phase. We consequently suggest a future adaptation
526 of the SAFY model by implementing variation with time for ELUE particularly after flowering.
527 The results also showed that the maximum GAI_{F2} value was a good indicator of the canopy
528 water and temperature stress. Thus the need of a temperature stress function like used into the
529 SAFY model should be questioned through further studies.

530 Finally, inter-annual variation in grain yields over the entire Formosat-2 data set of images (24 x
531 24 km²) was estimated using maize and sunflower and compared with grain yield statistics given
532 by the French Agricultural Statistics for the entire department of Haute-Garonne (6300 km²).
533 The SAFY model was able to correctly reproduce the inter-annual variation in the grain yield of
534 sunflower ($r^2 = 0.89$). In contrast, the inter-annual variation of maize grain yield was not
535 correctly reproduced because of the lack of spatial representativeness of our model simulations.

536 This study demonstrates the great potential for the use of high spatial and temporal resolution
537 remote sensing data for large-scale crop monitoring. Nevertheless, the high spatial resolution
538 was not fully exploited as simulations were carried out over homogenous unit. Future studies
539 could focus on analysing the intra-field variability by applying such approach at pixel level.
540 Future satellite missions such as Venµs (Dedieu et al. 2006) and Sentinel-2, which will provide
541 high spatial and temporal resolution images with a 4/5 days revisiting period and with a high

542 number of spectral bands (12/13 spectral bands), will offer new perspectives for such
543 applications.

544 ***Acknowledgements***

545 This work was made possible through the support of the European Commission (FEDER Interreg
546 IVa program, ref POCTEFA 08/34, Fluxpyr), the French Ministry in Charge of Research ("Réseau
547 Terre et Espace"), the Centre National de la Recherche Scientifique (CNRS), the Institut National
548 des Sciences de l'Univers (INSU), the Centre National d'Etudes Spatiales (CNES) and the Région
549 Midi-Pyrénées Council. We are very grateful to the farmers of Auradé and Lamothe and to
550 Michel Gay from E.I. Purpan for granting and facilitating our access to their fields. We also
551 express gratitude to Eric Martin from CNRM-GAME (Météo France) for providing the SAFRAN
552 meteorological data. We finally would like to thank Marie Weiss and Frédéric Baret from
553 EMMAH (INRA Avignon) for the support on CAN-EYE software. Special thanks to our technical
554 staff: Hervé Gibrin, Nicole Ferroni and Bernard Marciel.

555 **References**

- 556 Agreste (2011). La statistique Agricole. *Ministère de l'agriculture et de la pêche*.
557 <http://www.agreste.agriculture.gouv.fr>, last access: May 2011.
- 558 Andrade, F.H. (1995). Analysis of growth and yield of maize, sunflower and soybean grown at
559 Balcarce, Argentina. *Field Crops Research*, 41, 1-12.
- 560 Asrar, G., Fuchs, M., Kanemasu, E.T., & Hatfield, J.L. (1984). Estimating absorbed
561 photosynthetic radiation and leaf-area index from spectral reflectance in wheat. *Agronomy*
562 *Journal*, 76, 300-306.
- 563 Baillarin, S., Gigord, P., & O., H. (2008). Automatic Registration of optical images, a stake for
564 future missions: application to ortho-rectification, time series and mosaic products. *2008 Ieee*
565 *International Geoscience and Remote Sensing Symposium*, Vols 1-8, 928-931.
- 566 Baret, F., & Guyot, G. (1991). Potentials and limits of vegetation indexes for lai and apar
567 assessment. *Remote Sensing of Environment*, 35, 161-173.
- 568 Baret, F., Hagolle, O., Geiger, B., Bicheron, P., Miras, B., Huc, M., Berthelot, B., Nino, F.,
569 Weiss, M., Samain, O., Roujean, J.L., & Leroy, M. (2007). LAI, fAPAR and fCover CYCLOPES
570 global products derived from VEGETATION - Part 1: Principles of the algorithm. *Remote*
571 *Sensing of Environment*, 110, 275-286.
- 572 Baret, F., de Solan, B., Lopez-Lozano, R., Ma, K., & Weiss, M. (2010). GAI estimates of row
573 crops from downward looking digital photos taken perpendicular to rows at 57.5 degrees zenith

574 angle: Theoretical considerations based on 3D architecture models and application to wheat
575 crops. *Agricultural and Forest Meteorology*, 150, 1393-1401.

576 Basso, B., Ritchie, J.T., Pierce, F.J., Braga, R.P., & Jones, J.W. (2001). Spatial validation of crop
577 models for precision agriculture. *Agricultural Systems*, 68, 97-112.

578 Bastiaanssen, W.G.M., Molden, D.J., & Makin, I.W. (2000). Remote sensing for irrigated
579 agriculture: examples from research and possible applications. *Agricultural Water Management*,
580 46, 137-155.

581 Boote, K.J., Jones, J.W., & Pickering, N.B. (1996). Potential uses and limitations of crop models.
582 *Agronomy Journal*, 88, 704-716.

583 Brisson, N., Ruget, F., Gate, P., Lorgeau, J., Nicoullaud, B., Tayot, X., Plenet, D., Jeuffroy,
584 M.H., Bouthier, A., Ripoche, D., Mary, B., & Justes, E. (2002). STICS: a generic model for
585 simulating crops and their water and nitrogen balances. II. Model validation for wheat and maize.
586 *Agronomie*, 22, 69-92.

587 Brisson, N., Gary, C., Justes, E., Roche, R., Mary, B., Ripoche, D., Zimmer, D., Sierra, J.,
588 Bertuzzi, P., Burger, P., Bussiere, F., Cabidoche, Y.M., Cellier, P., Debaeke, P., Gaudillere, J.P.,
589 Henault, C., Maraux, F., Seguin, B., & Sinoquet, H. (2003). An overview of the crop model
590 STICS. *European Journal of Agronomy*, 18, 309-332.

591 Bsaibes, A., Courault, D., Baret, F., Weiss, M., Oliosio, A., Jacob, F., Hagolle, O., Marloie, O.,
592 Bertrand, N., Desfond, V., & Kzemipour, F. (2009). Albedo and LAI estimates from
593 FORMOSAT-2 data for crop monitoring. *Remote Sensing of Environment*, 113, 716-729.

594 Cabelguenne, M., Debaeke, P., & Bouniols, A. (1999). EPICphase, a version of the EPIC model
595 simulating the effects of water and nitrogen stress on biomass and yield, taking account of
596 developmental stages: validation on maize, sunflower, sorghum, soybean and winter wheat.
597 *Agricultural Systems*, 60, 175-196.

598 Casadebaig, P. (2008). Analyse et modélisation des interactions génotype - environnement -
599 conduite de culture : application au tournesol (*Helianthus annuus*). In, *Agrosystèmes et*
600 *développement territorial (AGIR)*. Toulouse.

601 Ceschia, E., Beziat, P., Dejoux, J.F., Aubinet, M., Bernhofer, C., Bodson, B., Buchmann, N.,
602 Carrara, A., Cellier, P., Di Tommasi, P., Elbers, J.A., Eugster, W., Gruenwald, T., Jacobs, C.M.J.,
603 Jans, W.W.P., Jones, M., Kutsch, W., Lanigan, G., Magliulo, E., Marloie, O., Moors, E.J.,
604 Moureaux, C., Olioso, A., Osborne, B., Sanz, M.J., Saunders, M., Smith, P., Soegaard, H., &
605 Wattenbach, M. (2010). Management effects on net ecosystem carbon and GHG budgets at
606 European crop sites. *Agriculture Ecosystems & Environment*, 139, 363-383.

607 Chern, J.S., Wu, A.M., & Lin, S.F. (2006). Lesson learned from FORMOSAT-2 mission
608 operations. *Acta Astronautica*, 59, 344-350.

609 Colombo, R., Bellingeri, D., Fasolini, D., & Marino, C.M. (2003). Retrieval of leaf area index in
610 different vegetation types using high resolution satellite data. *Remote Sensing of Environment*,
611 86, 120-131.

612 Courault, D., Bsaibes, A., Kpemlie, E., Hadria, R., Hagolle, O., Marloie, O., Hanocq, J.F.,
613 Olioso, A., Bertrand, N., & Desfonds, V. (2008). Assessing the potentialities of FORMOSAT-2

614 data for water and crop monitoring at small regional scale in South-Eastern France. *Sensors*, 8,
615 3460-3481.

616 Dedieu, G., Karnieli, A., Hagolle, O., Jeanjean, H., Cabot, F., Ferrier, P., & al., e. (2006).
617 VEN μ S: A joint Israel–French Earth Observation scientific mission with High spatial and
618 temporal resolution capabilities. In, *Second Recent Advances in Quantitative Remote Sensing*
619 *symposium*. Torrent.

620 Demarez, V., Duthoit, S., Baret, F., Weiss, M., & Dedieu, G. (2008). Estimation of leaf area and
621 clumping indexes of crops with hemispherical photographs. *Agricultural and Forest*
622 *Meteorology*, 148, 644-655.

623 Dolman, A.J., Noilhan, J., Durand, P., Sarrat, C., Brut, A., Piguet, B., Butet, A., Jarosz, N.,
624 Brunet, Y., Loustau, D., Lamaud, E., Tolk, L., Ronda, R., Miglietta, F., Gioli, B., Magliulo, V.,
625 Esposito, M., Gerbig, C., Korner, S., Glademard, R., Ramonet, M., Ciais, P., Neininger, B.,
626 Hutjes, R.W.A., Elbers, J.A., Macatangay, R., Schrems, O., Perez-Landa, G., Sanz, M.J., Scholz,
627 Y., Facon, G., Ceschia, E., & Beziat, P. (2006). The CarboEurope regional experiment strategy.
628 *Bulletin of the American Meteorological Society*, 87, 1367-+.

629 Dong, J.R., Kaufmann, R.K., Myneni, R.B., Tucker, C.J., Kauppi, P.E., Liski, J., Buermann, W.,
630 Alexeyev, V., & Hughes, M.K. (2003). Remote sensing estimates of boreal and temperate forest
631 woody biomass: carbon pools, sources, and sinks. *Remote Sensing of Environment*, 84, 393-410

632 Drouet, J.L., & Pages, L. (2003). GRAAL: a model of GRowth, Architecture and carbon
633 ALlocation during the vegetative phase of the whole maize plant - Model description and
634 parameterisation. *Ecological Modelling*, 165, 147-173.

635 Duchemin, B., Hadria, R., Erraki, S., Boulet, G., Maisongrande, P., Chehbouni, A., Escadafal, R.,
636 Ezzahar, J., Hoedjes, J.C.B., Kharrou, M.H., Khabba, S., Mougenot, B., Olioso, A., Rodriguez,
637 J.C., & Simonneaux, V. (2006). Monitoring wheat phenology and irrigation in Central Morocco:
638 On the use of relationships between evapotranspiration, crops coefficients, leaf area index and
639 remotely-sensed vegetation indices. *Agricultural Water Management*, 79, 1-27.

640 Duchemin, B., Maisongrande, P., Boulet, G., & Benhadj, I. (2008a). A simple algorithm for yield
641 estimates: Evaluation for semi-arid irrigated winter wheat monitored with green leaf area index.
642 *Environmental Modelling & Software*, 23, 876-892.

643 Duchemin, B., Hagolle, O., Mougenot, B., Benhadj, I., Hadria, R., Simonneaux, V., Ezzahar, J.,
644 Hoedjes, J., Khabba, S., Kharrou, M.H., Boulet, G., Dedieu, G., Er-Raki, S., Escadafal, R.,
645 Olioso, A., & Chehbouni, A.G. (2008b). Agrometeorological study of semi-arid areas: an
646 experiment for analysing the potential of time series of FORMOSAT-2 images (Tensift-
647 Marrakech plain). *International Journal of Remote Sensing*, 29, 5291-5300.

648 Durand, Y., Brun, E., Mérindol, L., Guyomarc'h, G., Lesaffre, B., & Martin, E. (1993). A
649 meteorological estimation of relevant parameters for snow models. In (pp. 65-71): *Annals of*
650 *Glaciology*.

651 Faivre, R., Leenhardt, D., Voltz, M., Benoît, M., Papy, F., Dedieu, G., & Wallach, D. (2004).
652 Spatialising crop models. *Agronomie*, 24, 205-217.

653 Fieuzal, R., Duchemin, B., Jarlan, L., Zribi, M., Baup, F., Merlin, O., Dedieu, G., Garatuza-
654 Payan, J., Watt, C., & Chehbouni, A. (2010). Combined use of optical and radar satellite data for
655 the monitoring of irrigation and soil moisture of wheat crops. (pp. 6207-6242).

656 Fjortoft, R., Lopes, A., Bruniquel, J., & Marthon, P. (1999). Optimal edge detection and edge
657 localization in complex SAR images with correlated speckle. *Ieee Transactions on Geoscience*
658 *and Remote Sensing*, 37, 2272-2281.

659 Flenet, F., Kiniry, J.R., Board, J.E., Westgate, M.E., & Reicosky, D.C. (1996). Row spacing
660 effects on light extinction coefficients of corn, sorghum, soybean, and sunflower. *Agronomy*
661 *Journal*, 88, 185-190.

662 Hadria, R., Duchemin, B., Baup, F., Le Toan, T., Bouvet, A., Dedieu, G., & Le Page, M. (2009).
663 Combined use of optical and radar satellite data for the detection of tillage and irrigation
664 operations: Case study in Central Morocco. *Agricultural Water Management*, 96, 1120-1127.

665 Hadria, R., Duchemin, B., Jarlan, L., Dedieu, G., Baup, F., Khabba, S., Oliosio, A., & Le Toan, T.
666 (2010). Potentiality of optical and radar satellite data at high spatio-temporal resolutions for the
667 monitoring of irrigated wheat crops in Morocco. *International Journal of Applied Earth*
668 *Observation and Geoinformation*, 12, S32-S37.

669 Hagolle, O., Dedieu, G., Mougenot, B., Debaecker, V., Duchemin, B., & Meygret, A. (2008).
670 Correction of aerosol effects on multi-temporal images acquired with constant viewing angles:
671 Application to Formosat-2 images. *Remote Sensing of Environment*, 112, 1689-1701.

672 Hagolle, O., Huc, M., Pascual, D.V., & Dedieu, G. (2010). A multi-temporal method for cloud
673 detection, applied to FORMOSAT-2, VEN μ S, LANDSAT and SENTINEL-2 images. *Remote*
674 *Sensing of Environment*, 114, 1747-1755.

675 Hutchinson, J.J., Campbell, C.A., & Desjardins, R.L. (2004). Some perspectives on carbon
676 sequestration in agriculture. In, *International Workshop on Contribution of Agriculture to the*
677 *State of Climate* (pp. 288-302). Ottawa, CANADA: Elsevier Science Bv.

678 Idbraim, S. (2009). Méthodes d'extraction de l'information spatiale et de classification en
679 imagerie de télédétection : Applications à la cartographie thématique de la région d'Agadir
680 (Maroc). In, *Sciences de l'Univers, de l'Environnement et de l'Espace* (p. 149). Toulouse:
681 Université Toulouse III - Paul Sabatier.

682 Jamieson, P.D., Porter, J.R., Goudriaan, J., Ritchie, J.T., van Keulen, H., & Stol, W. (1998). A
683 comparison of the models AFRCWHEAT2, CERES-wheat, Sirius, SUCROS2 and SWHEAT
684 with measurements from wheat grown under drought. *Field Crops Research*, 55, 23-44.

685 Kutsch, W.L., Aubinet, M., Buchmann, N., Smith, P., Osborne, B., Eugster, W., Wattenbach, M.,
686 Schrumpp, M., Schulze, E.D., Tomelleri, E., Ceschia, E., Bernhofer, C., Beziat, P., Carrara, A.,
687 Di Tommasi, P., Gruenwald, T., Jones, M., Magliulo, V., Marloie, O., Moureaux, C., Olioso, A.,
688 Sanz, M.J., Saunders, M., Sogaard, H., & Ziegler, W. (2010). The net biome production of full
689 crop rotations in Europe. *Agriculture Ecosystems & Environment*, 139, 336-345.

690 Lagarias, J.C., Reeds, J.A., Wright, M.H., & Wright, P.E. (1998). Convergence properties of the
691 Nelder-Mead simplex method in low dimensions. *Siam Journal on Optimization*, 9, 112-147.

692 Lecoecur, J., Poire-Lassus, R., Christophe, A., Pallas, B., Casadebaig, P., Debaeke, P., Vear, F., &
693 Guilioni, L. (2011). Quantifying physiological determinants of genetic variation for yield
694 potential in sunflower. SUNFLO: a model-based analysis. *Functional Plant Biology*, 38, 246-
695 259.

696 Lindquist, J.L., Arkebauer, T.J., Walters, D.T., Cassman, K.G., & Dobermann, A. (2005). Maize
697 radiation use efficiency under optimal growth conditions. *Agronomy Journal*, 97, 72-78.

698 Liu, J.G., Pattey, E., Miller, J.R., McNairn, H., Smith, A., & Hu, B.X. (2010). Estimating crop
699 stresses, aboveground dry biomass and yield of corn using multi-temporal optical data combined
700 with a radiation use efficiency model. *Remote Sensing of Environment*, 114, 1167-1177.

701 Lobell, D.B., Asner, G.P., Ortiz-Monasterio, J.I., & Benning, T.L. (2003). Remote sensing of
702 regional crop production in the Yaqui Valley, Mexico: estimates and uncertainties. *Agriculture
703 Ecosystems & Environment*, 94, 205-220.

704 Loseen, D., Mougin, E., Rambal, S., Gaston, A., & Hiernaux, P. (1995). A regional sahelian
705 grassland model to be coupled with multispectral satellite data .2. toward the control of its
706 simulations by remotely-sensed indexes. *Remote Sensing of Environment*, 52, 194-206.

707 Maas, S.J. (1993). Parameterized model of gramineous crop growth .1. leaf-area and dry mass
708 simulation. *Agronomy Journal*, 85, 348-353.

709 Monteith, J.L. (1977). Climate and efficiency of crop production in britain. *Philosophical
710 Transactions of the Royal Society of London Series B-Biological Sciences*, 281, 277-294.

711 Moulin, S., Bondeau, A., & Delecolle, R. (1998). Combining agricultural crop models and
712 satellite observations: from field to regional scales. *International Journal of Remote Sensing*, 19,
713 1021-1036.

714 Myneni, R.B., & Williams, D.L. (1994). On the relationship between FAPAR and NDVI. *Remote
715 Sensing of Environment*, 49, 200-211.

716 Pinter, P.J., Hatfield, J.L., Schepers, J.S., Barnes, E.M., Moran, M.S., Daughtry, C.S.T., &
717 Upchurch, D.R. (2003). Remote sensing for crop management. *Photogrammetric Engineering*
718 *and Remote Sensing*, 69, 647-664.

719 Prince, S.D. (1991). A model of regional primary production for use with coarse resolution
720 satellite data. *International Journal of Remote Sensing*, 12, 1313-1330.

721 Quintana-Segui, P., Le Moigne P., Durand Y., Martin E., Habets F., Baillon M., Canellas C.,
722 Franchisteguy L. & Morel S. (2008). Analysis of near-surface atmospheric variables : Validation of
723 the safran analysis over France, *Journal of Applied Meteorology and Climatology*, 47 (1), 92–107.

724 Scotford, I.M., & Miller, P.C.H. (2005). Applications of spectral reflectance techniques in
725 Northern European cereal production: A review. *Biosystems Engineering*, 90, 235-250.

726 Tucker, C.J., Vanpraet, C., Boerwinkel, E., & Gaston, A. (1983). Satellite remote-sensing of total
727 dry-matter production in the senegalese sahel. *Remote Sensing of Environment*, 13, 461-474.

728 Tucker, C.J., & Sellers, P.J. (1986). Satellite remote-sensing of primary production. *International*
729 *Journal of Remote Sensing*, 7, 1395-1416.

730 Varlet-Grancher, C., Bonhomme, R., Chartier, M., & Artis, P. (1982). Efficience de la conversion
731 de l'énergie solaire par un couvert végétal. In (pp. 3-26): Acta Oecologia/Oecologia Plantarum

732 Walthall, C., Dulaney, W., Anderson, M., Norman, J., Fang, H.L., & Liang, S.L. (2004). A
733 comparison of empirical and neural network approaches for estimating corn and soybean leaf
734 area index from Landsat ETM+ imagery. *Remote Sensing of Environment*, 92, 465-474.

735 Weiss, M., Baret, F., Leroy, M., Hautecoeur, O., Bacour, C., Prevot, L., & Bruguier, N. (2002).
736 Validation of neural net techniques to estimate canopy biophysical variables from remote sensing
737 data. *Agronomie*, 22, 547-553.

738 Wessels, K.J., Prince, S.D., Zambatis, N., Macfadyen, S., Frost, P.E., & Van Zyl, D. (2006).
739 Relationship between herbaceous biomass and 1-km(2) Advanced Very High Resolution
740 Radiometer (AVHRR) NDVI in Kruger National Park, South Africa. *International Journal of*
741 *Remote Sensing*, 27, 951-973.

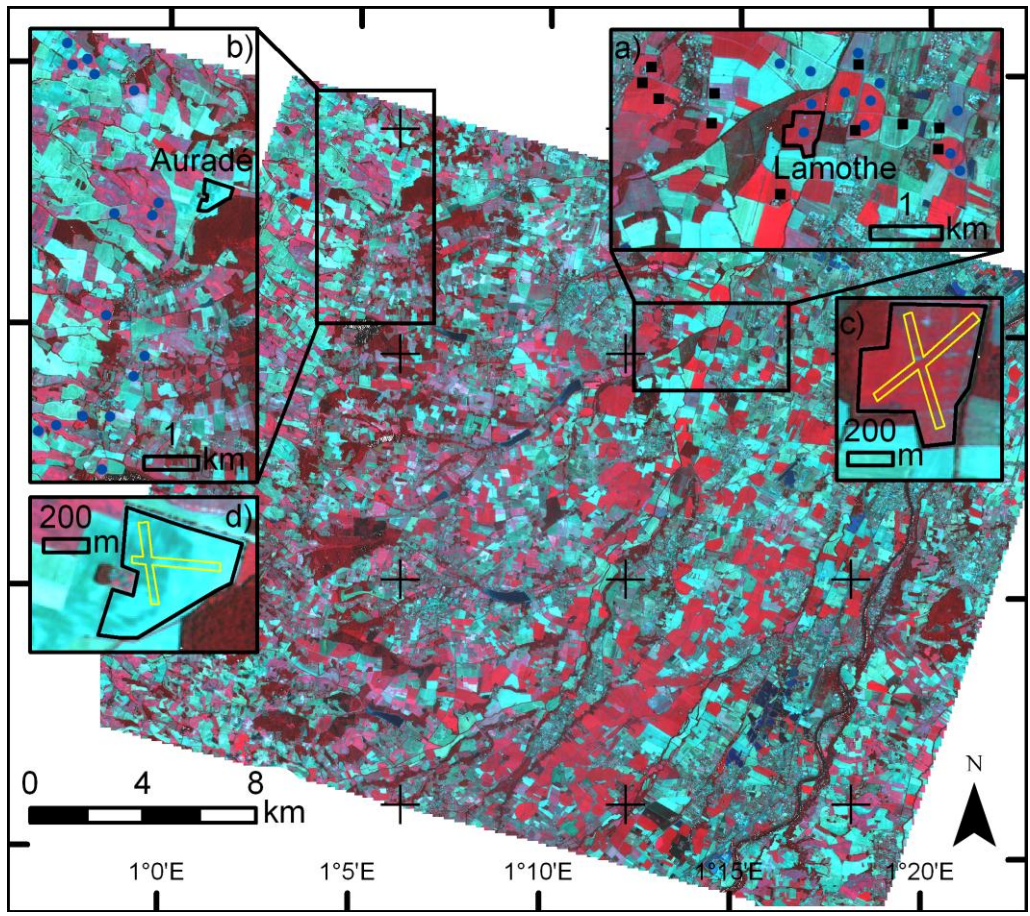
742 Wit de, A.J.W., Boogaard, H.L., & van Diepen, C.A. (2005). Spatial resolution of precipitation
743 and radiation: The effect on regional crop yield forecasts. *Agricultural and Forest Meteorology*,
744 135, 156-168.

745 Wylie, B.K., Harrington, J.A., Prince, S.D., & Denda, I. (1991). Satellite and ground-based
746 pasture production assessment in Niger - 1986-1988. *International Journal of Remote Sensing*,
747 12, 1281-1300.

748 Xevi, E., Gilley, J., & Feyen, J. (1996). Comparative study of two crop yield simulation models.
749 *Agricultural Water Management*, 30, 155-173.

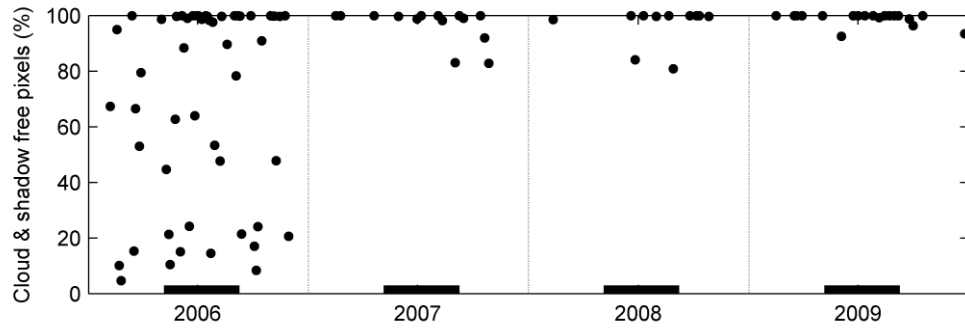
750

751 **Figures**



752
753 **Figure 1:** The study area as observed in a Formosat-2 image in July 2008. The areas where field data were collected are shown
754 in a) and b) frames; the black symbols indicate the locations of the elementary sampling units (11 ESUs near Lamothe), and
755 the blue disks indicate the fields for which the farmers provided grain yield data (12 fields near Lamothe, 16 fields near
756 Auradé). The so-called Lamothe (frame c) and Auradé (frame d) fields (delimited with black lines) are experimental fields that
757 belong to the CarboEurope-IP experiment; biomass measurements were performed along transects (in yellow). Black crosses
758 indicate the SAFRAN meteorological grid.

759

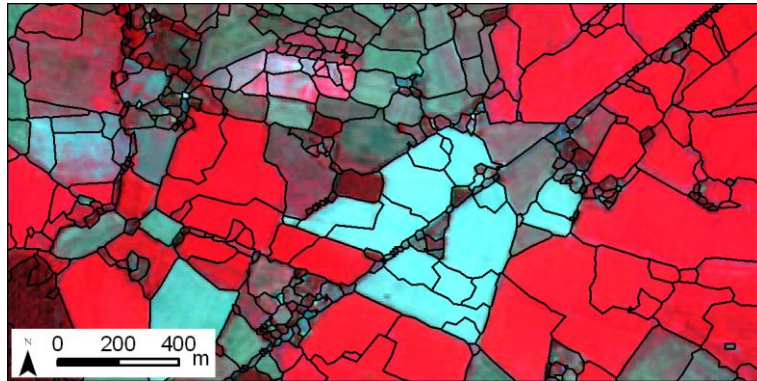


760

761 **Figure 2: Dates of acquisition of the Formosat-2 images with the corresponding percentage of cloud-free and shadow-free**
 762 **pixels. Thick black lines represent the standard summer crop-growing period (day of year 125 to 250).**

763

764

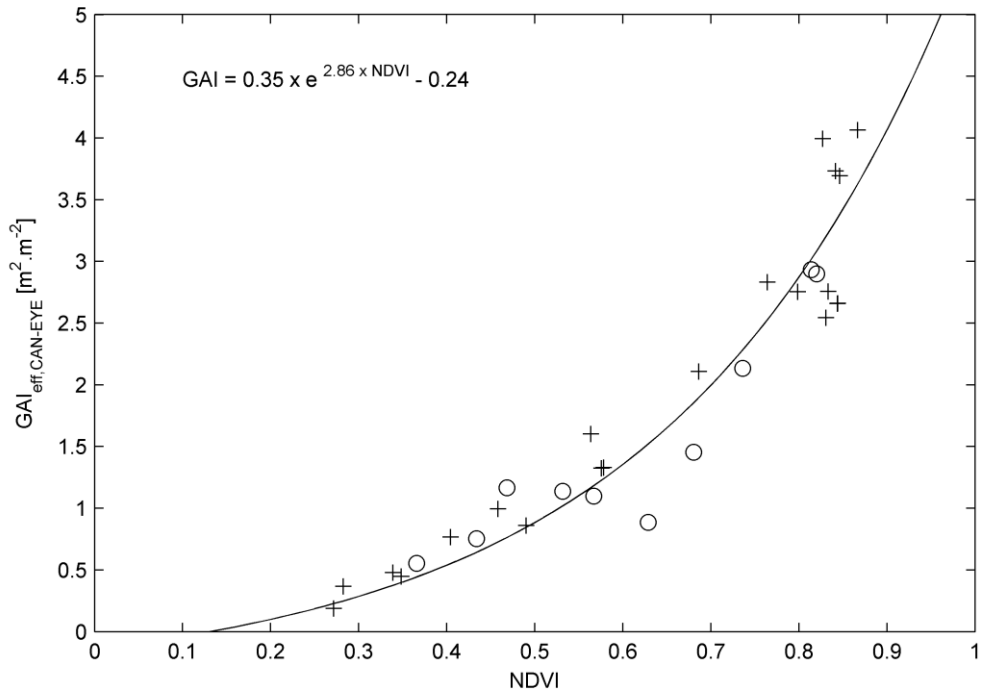


765

766 **Figure 3: Map of delimitation of Homogenous Unit (black lines). The background corresponds to a Formosat-2 image in July**

767 **2008, displayed using a false colour composite.**

768



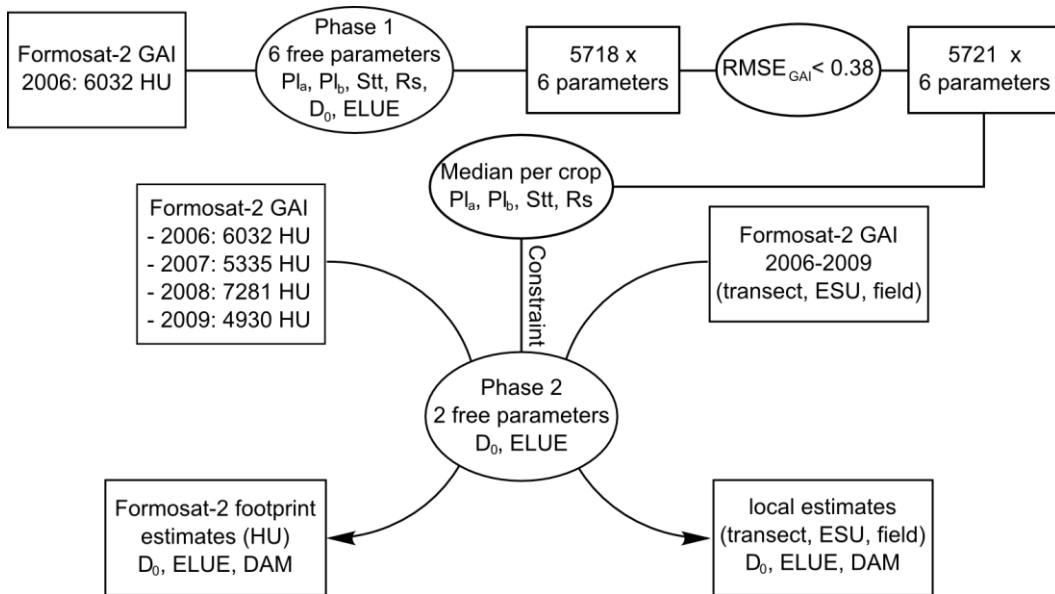
770

771 **Figure 4: Exponential law (black line) between the effective green area index ($GAI_{\text{eff,CAN-EYE}}$) and Formosat-2 NDVI. $GAI_{\text{eff,CAN-EYE}}$**

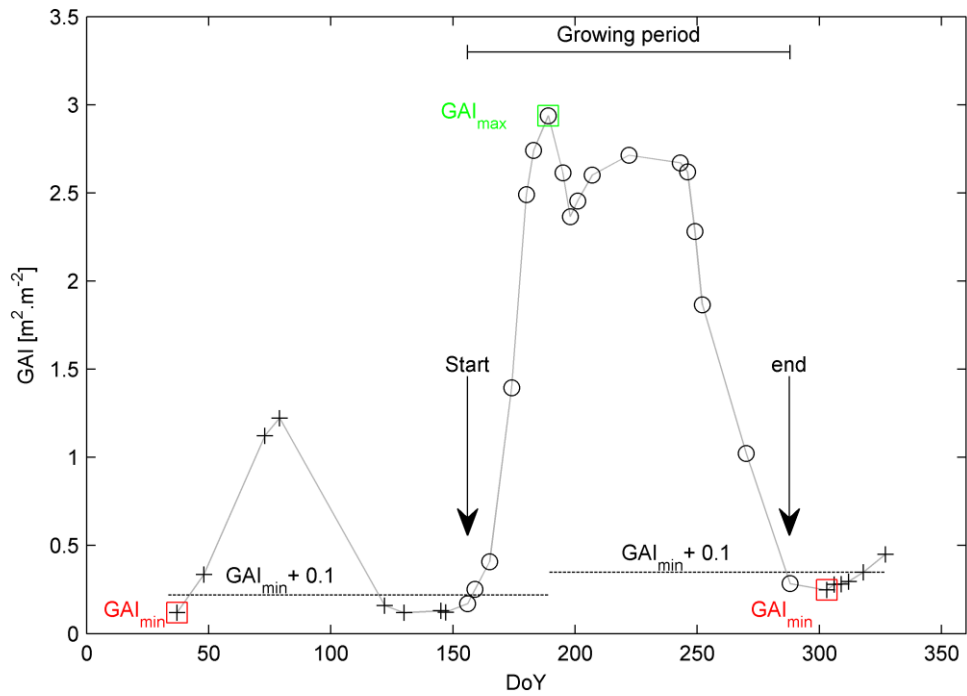
772 **were collected per ESU and NDVI were averaged on a 3×3 pixels windows centred on the ESU. Pluses and circles indicate**

773 **maize and sunflower crops, respectively.**

774



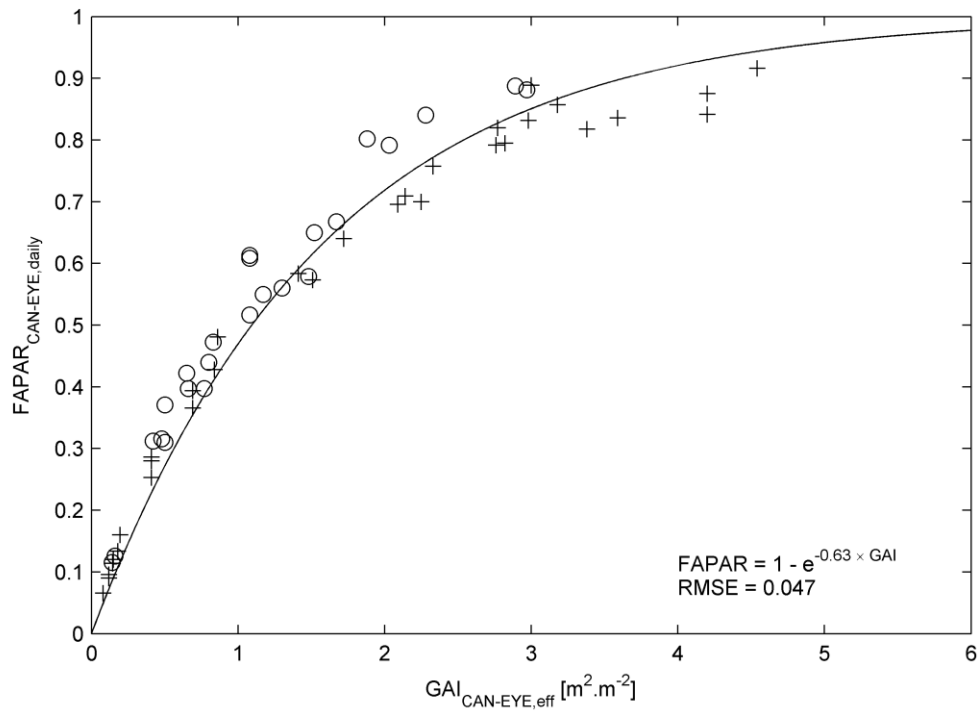
775
 776 **Figure 5: Description of the two phases of the calibration. Phase 1 and 2 describes the calibration of the crop-specific**
 777 **parameters and the field-specific parameters, respectively.**



778

779 **Figure 6: Example of the delimitation of the growing season on a Formosat-2 GAI time series for maize. The dashed line**
 780 **indicates the normal law fitted on the GAI time series. The maximum GAI is framed in green and the two minimum GAI (from**
 781 **each side) are framed in red. The horizontal dashed lines indicate the bare soil thresholds used to detect the start and the end**
 782 **of the growing period. Circles and crosses indicate, respectively, selected and non-selected data acquired within the growing**
 783 **period.**

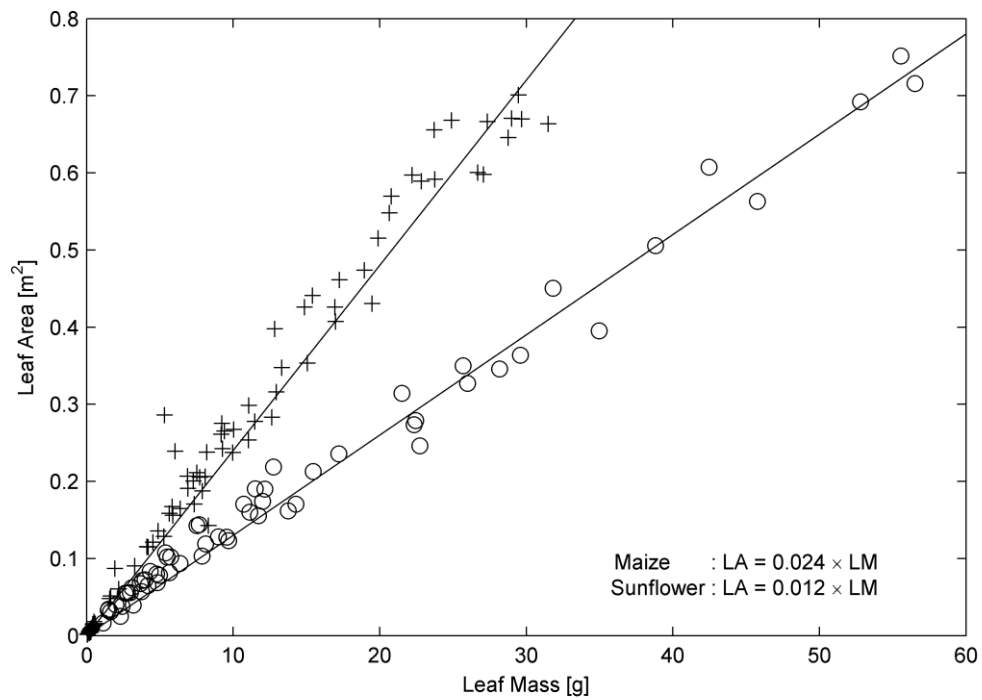
784



785

786 **Figure 7: Relationship between the daily fraction of absorbed photosynthetically active radiation ($FAPAR_{daily,CAN-EYE}$) and**
 787 **effective green area index ($GAI_{eff,CAN-EYE}$) derived from the hemispherical photographs. Pluses and circles indicate maize and**
 788 **sunflower crops, respectively.**

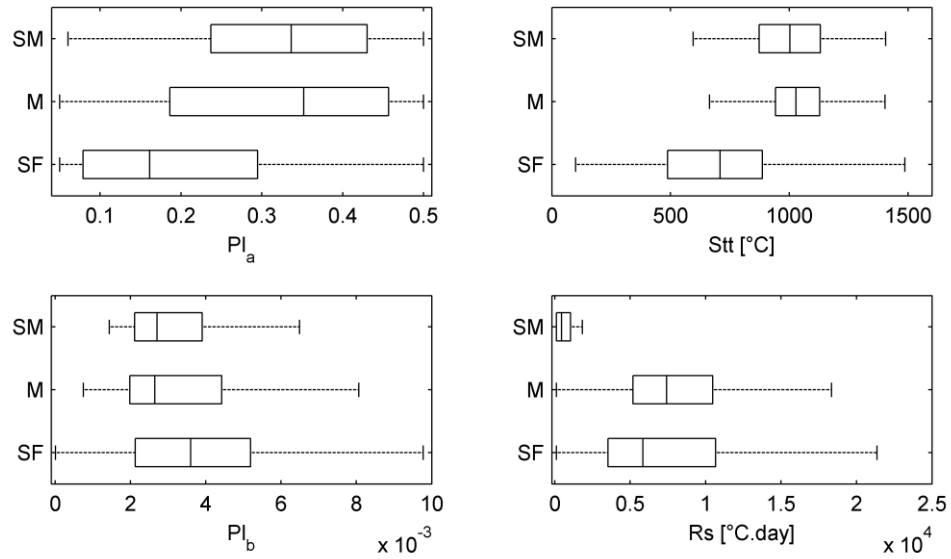
789



790

791 **Figure 8: Relationship between leaf area (LA) and leaf mass (LM) estimated from destructive measurements. Pluses and**
 792 **circles indicate maize and sunflower crops, respectively. The slopes of the solid lines correspond to the SLA ($m^2 \cdot g^{-1}$) values.**

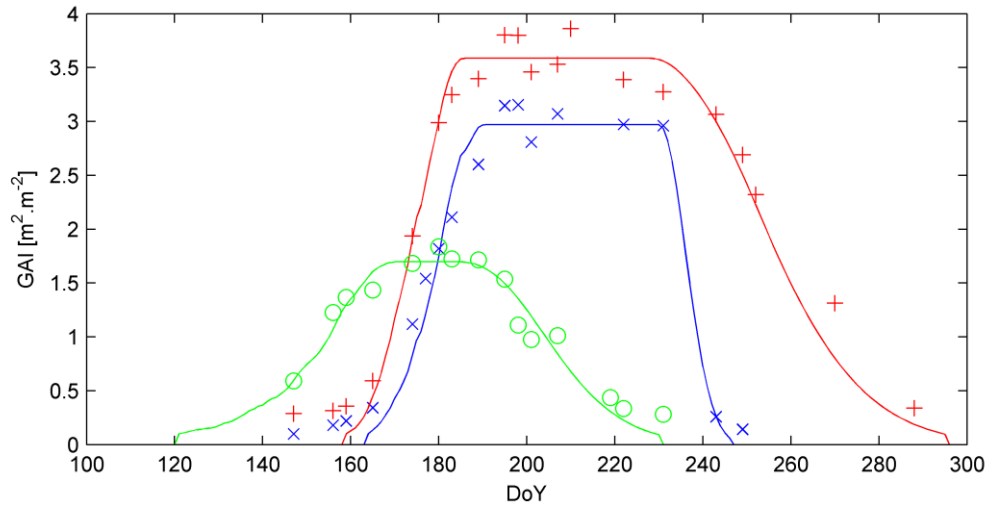
793



794

795 **Figure 9: Distributions of crop-specific parameters of maize (grain: M and Silage: SM) and sunflower (SF) based on phase 1 of**
 796 **the calibration applied on the 5721 HU of the 2006 Formosat-2 data set (1980 for grain maize, 97 for silage maize and 3644**
 797 **for sunflower). Lower and upper quartiles and median values are presented. The whiskers (lines extending from each end of**
 798 **the boxes) show the extent of the rest of the data, excluding outliers (not shown).**

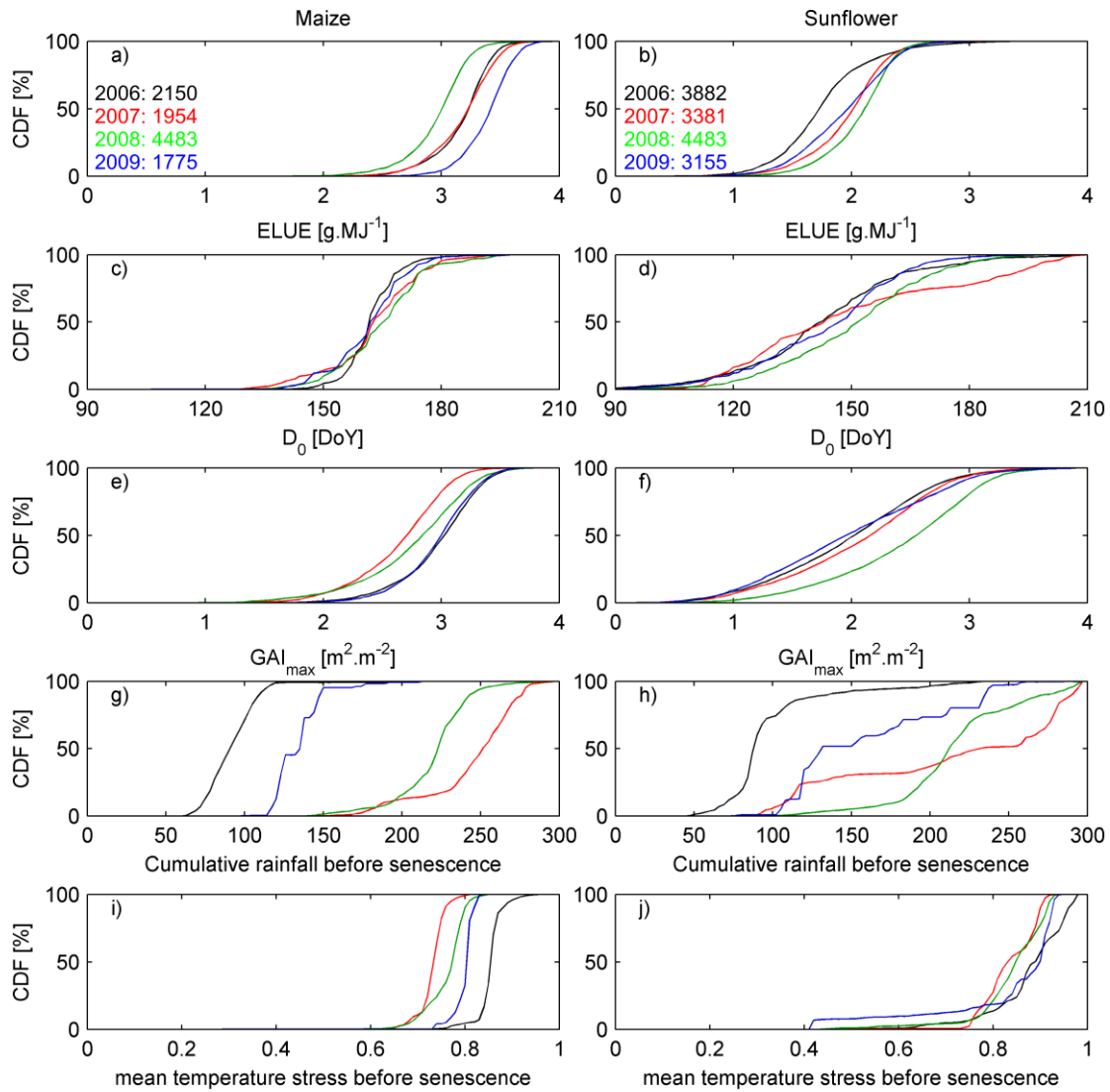
799



800

801 **Figure 10: Example of three 2006 Formosat-2 GAI time series. Red pluses, blue crosses and green circles indicate grain maize,**
 802 **silage maize and sunflower, respectively. Full lines show the SAFY simulations.**

803



804

805 **Figure 11: Cumulative distribution function (CDF) of ELUE (a and b), D₀ (c and d) and maximum GAI (GAI_{max}, e and f) simulated**

806 **for maize (left column) and sunflower (right column) in 2006 (black), 2007 (red), 2008 (green) and 2009 (blue) over the whole**

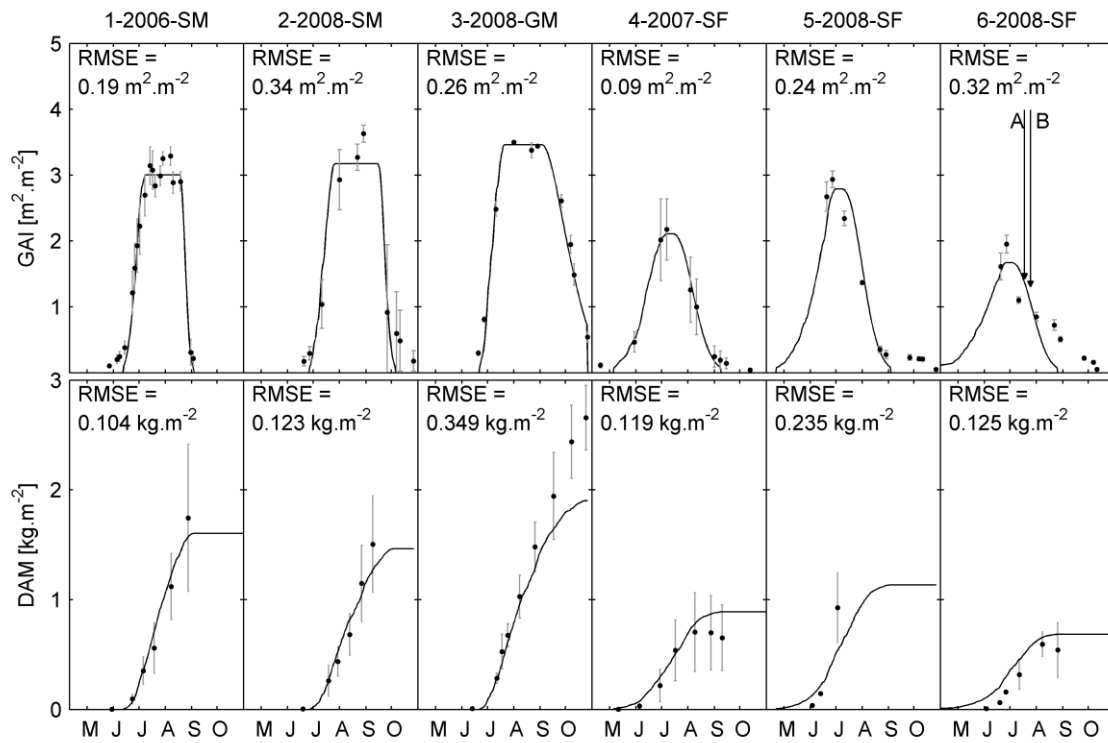
807 **Formosat-2 footprint. The rainfall (g and h) was cumulated from 30 days before emergence to the start of the senescence.**

808 **The mean temperature stress (i and j) was cumulated from emergence to the start of the senescence. The amount of data**

809 **used is shown in a and b.**

810

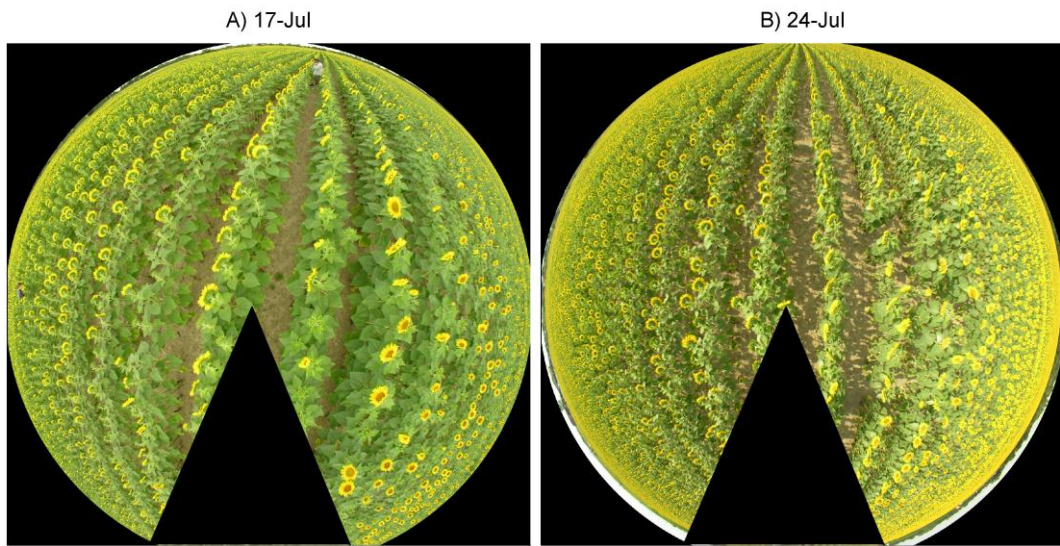
811



812

813 Figure 12: Green area index (GAI) and dry aboveground mass (DAM) simulated (lines) and measured (dots) over 6
814 experimental fields for the period 2006-2008. M: maize, SM: silage maize and SF: sunflower. Grey error bars on GAI and DAM
815 correspond to the standard deviation computed from the pixels (GAI) and the measurements (DAM) performed either over
816 the transects (cases 1, 2 and 4) or the ESUs (case 3, 5 and 6). A and B, mentioned for case 6, refer to the hemispherical
817 photographs shown in Fig. 13.

818

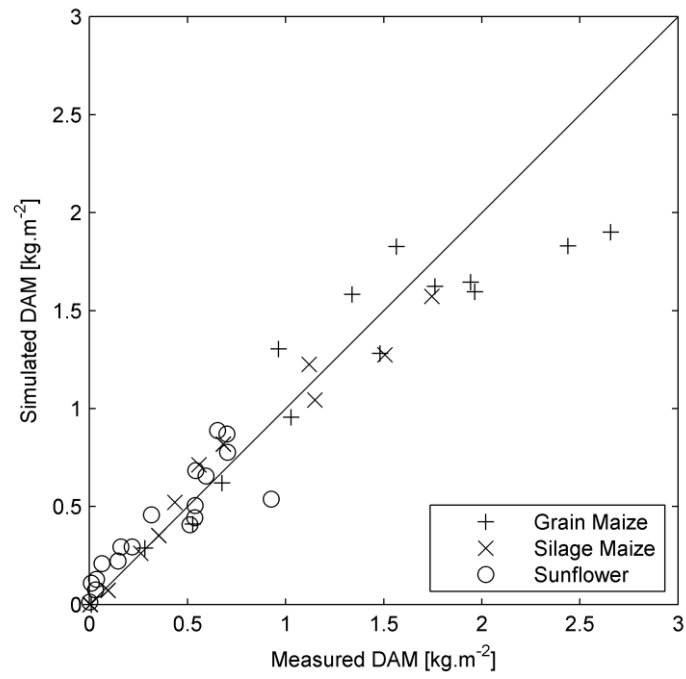


819

820 **Figure 13: Hemispherical photographs taken in 2008 on July 17 (A) and July 24 (B) over the ESUs corresponding to case 6 of**

821 **Fig. 12.**

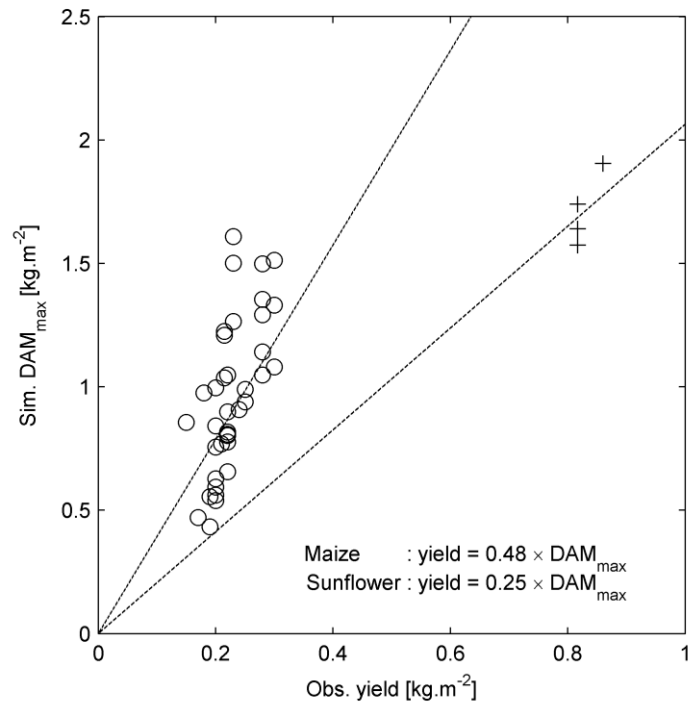
822



823

824 **Figure 14: Comparison between the simulated and measured dry aboveground mass (DAM) over all of the experimental fields**
 825 **for the period 2006-2009.**

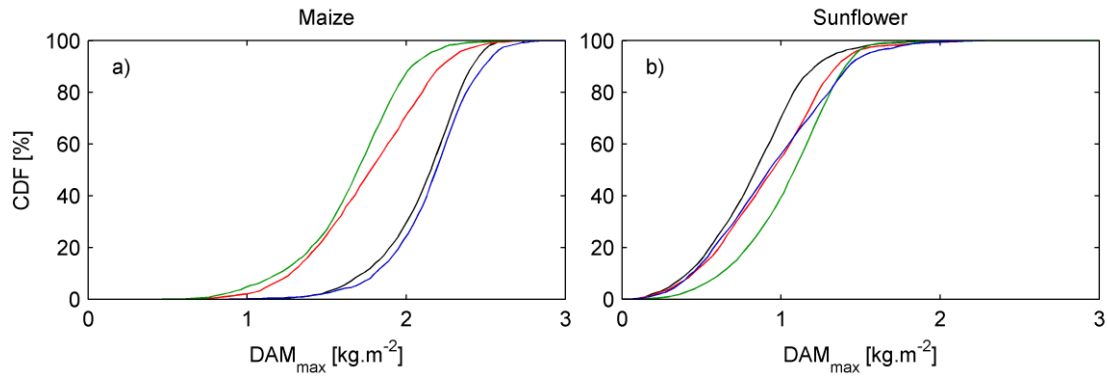
826



827

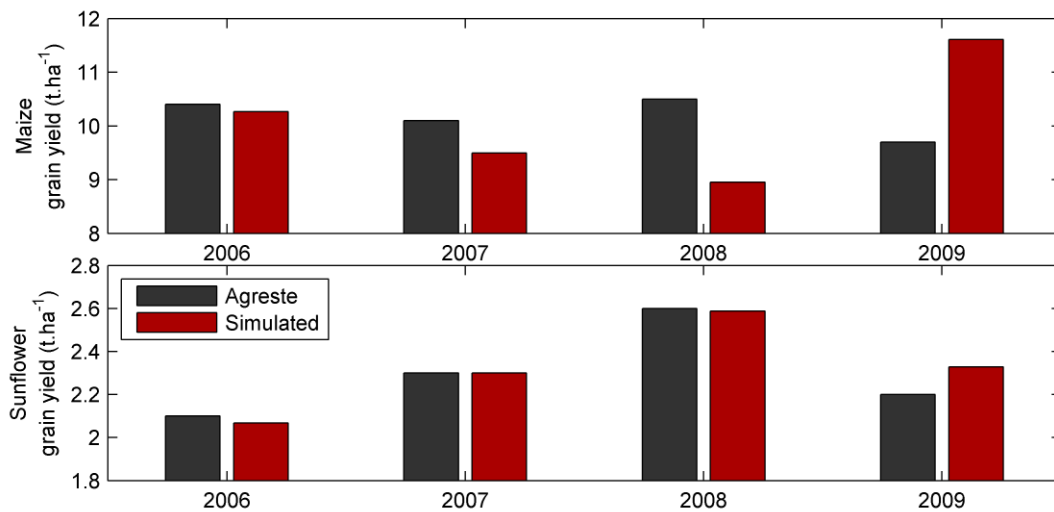
828 **Figure 15: Relationship between simulated maximum dry aboveground mass (DAM_{max}) and grain yields in 2006, 2007 and**
 829 **2008, provided by farmers for 28 maize (+) and sunflower (o) crops. The slopes of the dashed lines correspond to the mean**
 830 **harvest index.**

831



832
 833 **Figure 16: Cumulative distribution function (CDF) of maximum dry aboveground mass (DAM_{max}) simulated for maize (a) and**
 834 **sunflower (b) in 2006 (black), 2007 (red), 2008 (green) and 2009 (blue) over the entire Formosat-2 footprint. The amount of**
 835 **data used is shown in Fig. 11 a and b.**

836



837
 838 **Figure 17: Comparison of the four-year grain yield (in $t \cdot ha^{-1}$) obtained from Agreste (2011) for the French department of**
 839 **Haute-Garonne and the yield simulated for the study area.**

840

841

842 **Tables**

843 **Table 1:** In situ measurements data description, including crop type, year of in situ measurements, and number of data
 844 collected for GAI, FAPAR and DAM. The sampling scheme is given in the two last columns: ESU (with the number of sampled
 845 field under bracket) or transect (Lamothe and Auradé). GAI and FAPAR were estimated from hemispherical photographs and
 846 DAM was estimated from destructive measurements.

Crop type	Year	GAI / FAPAR	DAM
Maize	2006		Lamothe: 6
	2008	ESU (3): 23	ESU (1): 9
			Lamothe: 6
	2009		ESU (5): 5
Sunflower	2007		Auradé: 7
	2008	ESU (2): 19	ESU (2): 9
			2009

847

848

849 **Table 2: List of the SAFY input parameters and initial values estimated from the literature for ϵ_C , T_{min} , T_{opt} , T_{max} , β and DAM_0 ,**
 850 **from measurements of K_{ext} and SLA from the calibration procedure for the crop specific (PI_a , PI_b , Rs , Stt) and field specific (D_0 ,**
 851 **ELUE) parameters.**

Parameter type and name	Notation	Unit	Range	Grain Maize	Silage Maize	Sunflower
<i>Constant (literature)</i>						
Climatic efficiency	ϵ_C	-		0.48*	0.48*	0.48*
Initial dry aboveground mass	DAM_0	$g.m^{-2}$		4.2	4.2	6.9
Temperature for growth [Minimal, Optimal, Maximal]	$T_{min}, T_{opt}, T_{max}$	$^{\circ}C$		[8 30 45] ⁺	[8 30 45] ⁺	[8 28.5 42] [‡]
Polynomial degree	β	-		2	2	3
<i>Constant (measured)</i>						
Light-interception coefficient	K_{ext}	-		0.63	0.63	0.63
Specific leaf area	SLA	$m^2.g^{-1}$		0.024	0.024	0.012
<i>Calibrated (Crop-specific)</i>						
Partition-to-leaf function: par a	PI_a	-	[0.05 0.5]	0.35	0.34	0.13
Partition-to-leaf function: par b	PI_b	-	[10^{-5} 10^{-2}]	0.0026	0.0027	0.0033
Rate of senescence	Rs	$^{\circ}C.day$	[0 10^5]	7410	457	5787
Temperature sum for senescence	Stt	$^{\circ}C$	[0 2000]	1028	1002	713
<i>Calibrated (Field-specific)</i>						
Day of plant emergence	D_0	DoY	[90 250]			
Effective light-use efficiency	ELUE	$g.MJ^{-1}$	[0.5 6]			

* Varlet-Grancher et al. (1982)

+ Drouet and Pages (2003)

‡ Stics website (http://www.avignon.inra.fr/agroclim_stics/)

852
853

854

855 **Table 3: Statistics derived from the comparison of the SAFY simulated and the measured dry aboveground mass (DAM).**

	Maize	Sunflower	All crops
N	26	18	44
RMSE (kg.m ⁻²)	0.252	0.145	0.215
RRMSE (%)	24.67	39.11	28.44
Bias (kg.m ⁻²)	-0.070	0.049	-0.021
r ²	0.91	0.78	0.92

856

857

859 ***Appendix 1: Overview of the SAFY model.***

860 The simple algorithm for yield estimates (SAFY, Duchemin et al. 2008a) is a daily time-step
861 model that simulates time series of leaf area index (LAI) and dry aerial mass (DAM) from the air
862 temperature (T_a) and the global incoming radiation (R_g). The simulations begin on the plant
863 emergence day (D_0). D_0 depends on agricultural practices (in particular sowing date and depth)
864 and on the pedoclimatic conditions and constrains the phase of the LAI time course.

865 Daily DAM production (Δ_{DAM}) is calculated through the approach of Monteith (1977, Eq. 2) using
866 an effective light-use efficiency (ELUE), a daily temperature stress factor (F_T) and the daily
867 photosynthetically active radiation absorbed by plants (APAR). The ELUE expresses the
868 conversion of the APAR into DAM. It is supposed to account for all agri-environmental stresses,
869 such as water and nitrogen supplies, except for temperature. It constrains the amplitude of the
870 GAI time course. The temperature stress function is a classical Polynomial (Eq. 3) of β Degree
871 defined by an optimal daily mean air temperature (T_{opt}) for maximum crop functioning and two
872 extreme temperatures (T_{min} and T_{max}) beyond which the plant growth stops (after Brisson et al.
873 2003). The APAR (Eq. 4) is computed using the daily incoming global radiation (R_g), the climatic
874 efficiency (ϵ_c) and the fraction of the photosynthetically active portion of solar radiation
875 absorbed by green plants (FAPAR). In the SAFY model, the FAPAR is estimated using Beer's law
876 (Eq. 5), where k_{ext} defines the light-extinction coefficient (Monsi and Saeki 1953).

877
$$\Delta_{DAM} = ELUE \times F_T(T_a) \times APAR \quad (2)$$

$$\begin{cases}
F_T(Ta) = 1 - \left(\frac{T_{opt} - Ta}{T_{opt} - T_{min}} \right)^\beta & \text{if } T_{min} < Ta < T_{opt} \\
F_T(Ta) = 1 - \left(\frac{T_{opt} - Ta}{T_{opt} - T_{max}} \right)^\beta & \text{if } T_{max} > Ta > T_{opt} \\
F_T(Ta) = 0 & \text{if } Ta < T_{min} \text{ OR } Ta > T_{max}
\end{cases} \quad (3)$$

$$APAR = FAPAR \times \varepsilon_C \times Rg \quad (4)$$

$$FAPAR = 1 - e^{-k_{ext} \times LAI} \quad (5)$$

881 During plant growth, a fraction of the daily plant DAM production is partitioned to the dry leaf
882 biomass. This fraction is calculated using the partition-to-leaf function PI (Eq. 6, after Maas
883 1993), which varies from 0 to 1. PI is a function of the daily air temperature cumulated from
884 plant emergence (SMT: sum of temperature, Eq. 7) and two parameters: PI_a and PI_b . It should be
885 noted that $(1 - PI_a)$ defines the rate of biomass allocation to leaves at plant emergence. Daily
886 leaf mass production ($\Delta_{DAM} \times PI$) is converted into daily leaf area growth (Δ^+_{LAI}) based on the
887 specific leaf area (SLA, Eq. 8). Leaf senescence (Δ^-_{LAI}) begins when the SMT reaches a given
888 threshold (Stt, sum of temperature for senescence). It is modelled by a function (Eq. 9) based on
889 the rate of senescence coefficient (Rs). The LAI is updated from the balance of Δ^+_{LAI} and Δ^-_{LAI} (Eq.
890 10).

$$PI = 1 - PI_a \times e^{PI_b \times SMT} \quad (6)$$

$$SMT = \sum_{D_0}^t (Ta_t - T_{min}) \cdot dt \quad (7)$$

893 If $PI > 0$, $\Delta_{LAI}^+ = \Delta_{DAM} \times PI \times SLA$ (8)

894 If $SMT > Stt$, $\Delta_{LAI}^- = LAI \times \frac{SMT - Stt}{Rs}$ (9)

895 $LAI_t = LAI_{t-1} + \Delta_{LAI}^+ - \Delta_{LAI}^-$ (10)